D.Ph.II/MFL/ik PH.I/COM-69-37

To: Members of the Electronics Experiments Committee

From: M. Ferro-Luzzi, J.M. Perreau, T. Ypsilantis - CERN
G. Bizard, Y. Déclais, J. Duchon, J. Séguinot - University of Caen, France
G. Valladas, CEN, Saclay
C. Bricman, I.I.S.N., Bruxelles.

Subject: Appendix to "Proposal to measure the differential cross section of K^-n elastic scattering between ~ 1 and ~ 2 GeV/c".

I. Introduction

This note presents further explanations and answers the questions raised on the feasibility and usefulness of the experiment proposed in PH.I/COM-69-21 of May 20th, 1969.

The subject is divided into three parts: in section II we shall review the situation concerning the analysis of the $\bar{K}N$ interaction, in section III arguments will be presented supporting the use of the deuteron as a free nucleon target, and finally, in section IV, some technical aspects will be re-discussed.

II. Status of the $\bar{K}N$ partial wave analysis

An exhaustive discussion on this subject, including a complete series of references to the work done, can be found in the Rapporteur's Talk on strange baryon resonances at the Lund 1969 Conference on High Energy Physics[1]. We will not attempt to repeat or summarize here the content of the above Rapporteur's Talk. What we try instead is to present a somewhat detailed picture of

what goes on behind the curtain, i.e. what is the actual work that is done in order to interpret the experimental results.

Let us only recall that the main accomplishment of this field of study during the last few years has been the build-up of a consistent picture of the baryon multiplet structure within, for example, the SU(3) framework. A total of 3 singlets, 3 decuplets and 4 octets appears to be reasonably well established and - what is more - quantitatively consistent. This means that the members of the multiplets have: (a) the correct masses, (b) an established and identical spin-parity, (c) partial widths in agreement with the requirements of unique coupling constants. All this is not trivial, because it demands a correct assignment of each individual member of the multiplet as far as its angular and decay properties are concerned. We are far away from the rudimentary stage of only a few years past, when the discovery of a new resonant state was by itself a cause for rejoice.

Turning now to our subject, let us refer to fig. 1 that shows the 4 established octets and let us inspect where does the $\bar{K}N$ partial wave analysis come in and how. The S = -1 hyperons are denoted by their customary symbols (Λ for isospin 0, Σ for isospin 1) followed by their mass. The basic knowledge on these hyperons (and consequently their attribution to the specific multiplets of fig. 1) rests almost entirely on the partial wave analyses that will be described below. The outcome of these analyses, when successful, is the determination of mass, width, branching ratios, spin, parity and resonant phases. Usually this implies different analyses performed separately on the various available two-body channels. In what follows we will concentrate on the elastic channel; very similar approaches have been used when dealing with

the other reactions.

The interaction is described[2] by the scattering amplitudes f (the non-spin-flip term) and g (the spin-flip term). These contain the partial wave amplitudes $T_\ell^\pm$ (ℓ denotes the orbital angular momentum, + and - refer to a total angular momentum $J = \ell + \frac{1}{2}$ and $J = \ell - \frac{1}{2}$ respectively) as follows:

$$f = \lambda \Sigma_\ell \left[(\ell + 1)\, T_\ell^+ + \ell T^- \right] P_\ell (\cos\theta) \qquad (1)$$

$$g = i\lambda \Sigma_\ell \left[T_\ell^+ - T_\ell^- \right] P_\ell^1 (\cos\theta) \qquad (2)$$

The scattering amplitudes are then related to the observables (differential cross section and polarization) through

$$d\sigma/d\Omega = |f|^2 + |g|^2 \qquad (3)$$

$$\vec{p}(d\sigma/d\Omega) = 2\underline{\mathrm{Re}}(f^* g)\, \vec{n} \qquad (4)$$

Solving equations (3) and (4) with respect to $T_\ell^\pm$ is the purpose of the partial wave analysis. The quantities to be determined are complex and are frequently described by means of phase shifts ($\delta_\ell^\pm$) and absorption parameters ($\eta_\ell^\pm$):

$$T_\ell^\pm = (\eta_\ell^\pm e^{2i\delta_\ell^\pm} - 1)/2i \qquad (5)$$

In what follows we prefer to represent the amplitudes by means of their real and imaginary parts. The amplitudes will then be shown on a complex plane, where the energy dependence will be apparent from the trajectories described.

Two distinct approaches can be followed when trying to solve the problem. It is mainly the status of the experimental knowledge that determines which one to choose. There are, in

addition, intermediate situations where a mixture of the two methods can be adopted. We shall refer to these methods as the "energy - dependent" and the "energy -independent" approach.

Let us consider the K^-p elastic scattering. This reaction involves two isospin states, 0 and 1; thus, for a given set of ℓ and J, there will be two amplitudes, $T_{\ell,J}(I=0)$ and $T_{\ell,J}(I=1)$. Let us further assume that the interaction does not involve angular momenta larger than J = 5/2 (this is indeed the case for incident momenta below ~ 1 GeV/c). Then the number of amplitudes to be determined is 12. In spectroscopic notations (the first subscript referring to the isospin, the second to twice the angular momentum J) they are: S_{01}, S_{11}, P_{01}, P_{11}, P_{03}, P_{13}, D_{03}, D_{13}, D_{05}, D_{15}, F_{05}, F_{15}. At each energy there will be 12 x 2 = 24 real numbers to be determined. So as to evaluate how much experimental information is available when solving for the above quantities, it is convenient(*) to represent the results of the measurements under the form of a series expansion in appropriate polynomials of the scattering angle Θ. Thus, the differential cross sections $d\sigma/d\Omega$ will be expanded in Legendre polynomials:

$$d\sigma/d\Omega = \lambda\!\!\!^{-2} \sum_n A_n P_n(\cos\Theta) \qquad (6)$$

(*) In practice - and depending on the quality of the data - it is usually more meaningful to deal directly with the differential cross sections or polarizations as determined angle by angle. This may allow a better determination of the unknown quantities but does not change the above considerations.

and the polarization measurements $\vec{P}(d\sigma/d\Omega)$ in first-associated Legendre polynomials:

$$\vec{p}(d\sigma/d\Omega) = \vec{n}\,\lambda^2 \sum B_n P_n^1(\cos\theta) \qquad (7)$$

These expansions, in view of the above assumption on J, do not need to be carried further than the 5th order. It follows that a measurement of $d\sigma/d\Omega$ is equivalent to the knowledge of 6 coefficients (A_0 to A_5) and $\vec{P}(d\sigma/d\Omega)$ to 5 coefficients (B_1 to B_5). A comparison of equations (6) and (7) with (1) and (4) provides, next, a set of algebraic relations between the coefficients A_n and B_n and the partial wave amplitudes listed above. In our case, there will be 5 + 6 = 11 relations for a total of 24 unknowns at each energy. The problem is clearly non-determined. Let us notice, in passing, that the system would still be undetermined even if we had an equal number of relations and equations. In effect, the equations in question are bilinear and thus are not uniquely solvable. It is however easier to choose a "reasonable" set of solutions out of a few than out of many.

There are two ways of circumventing this undesirable situation. One is to measure some other quantity connected with our amplitudes. The other is of trying to guess the energy dependence of the amplitudes so as to relate the measurements made at different energies, thereby effectively increasing the number of useful relations.

The second method is clearly the cheaper one (requiring only some imagination) particularly in the early stage of the study, when the measurements are necessarily limited. This is what has been done below ~ 1 GeV/c, although in a slightly modified situation. Here the polarization is not yet available (due to serious experimental

difficulties) and the 5 relations originating from this measurement are missing. On the other hand, 6 other coefficients can instead be exploited, derived from the measurement of $d\sigma/d\Omega$ for the charge-exchange reaction $K^- p \to \bar{K}^0 n$. The latter contains the same amplitudes as $K^- p \to K^- p$ but in a different isospin combination. In addition, the optical theorem helps with two more relations in those regions where σ_0 and σ_1 (the isospin 0 and 1 total $\bar{K}N$ cross sections) have been measured[3,4,5]. Thus 14 equations are available versus 24 unknowns. An energy parametrization of each amplitude increases the amount of unknowns but - as long as the number of parameters per wave is kept to a sensible level - the gain achieved is remarkable. In the region below ~ 1 GeV/c the measurements have been done[6,7,8,9] with an average momentum spacing of ~ 20 MeV/c. If each amplitude is attributed 2 parameters to describe its energy dependence over, say, 200 MeV/c, this means a total of 2 x 24 = 48 parameters versus 14 x 10 = 140 data points. The parametrization may or may not be adequate, but the system is solvable and most ambiguities can be easily removed.

Without entering into the details of the search, a consistent and satisfactory solution[10,11,12,13,14] has been found in this way by means of a convenient dosage of the number of parameters, the type of parametrization ("resonant", "background", a mixture of the two, scattering-length approximation, etc....), the number and accuracy of the data and the energy interval examined. Fig. 2 gives an idea of the quality of the agreement that can be achieved between the measured and predicted coefficients[12]. The solution itself is shown in Fig. 3. The purpose of this figure is to give the general behaviour of the amplitudes; in reality, the solutions obtained by the different groups, although joining together and being in excellent agreement with each other, are not

as smooth and continuous as drawn here. The resonant amplitudes appear as circles (since they have been parametrized as Breit-Wigner resonances); the other amplitudes exhibit a "background" behaviour although, of course, it cannot be excluded at this stage that more structure will be detected when better parametrizations and more accurate measurements will be available.

Let us now turn to the so-called "energy-independent" approach where, given the necessary ingredients, there should be no need to invoke unnatural and necessarily inaccurate parametrizations (one still needs to invoke some artificial "continuity" requirement which may bias the type of solution obtained, but this is admittedly a minor point when compared to the drastic assumptions of the energy - dependent analysis). In order to tackle the problem, one needs to add to the above 14 relations some other independent measurement so as to reach - and possibly exceed - the required number of at least 24 relations between the 24 amplitudes. In principle one can recur to any of the following measurements: (a) polarization of the proton in $K^-p \to K^-p$ (5 relations), (b) polarization of the neutron in $K^-p \to \bar{K}^0n$, (5 relations), (c) differential cross section of the pure isospin 1 reaction $K^-n \to K^-n$ or, alternatively, $\bar{K}^0p \to \bar{K}^0p$ (6 relations); (d) polarization of the recoil nucleon of the reactions mentioned in (c) (5 relations).

Of these, below ~ 1 GeV/c, only (c) is available and in a statistically very limited way[15]. Fig. 4 illustrates the level of precision achieved in this measurement. We are still below the required set of relations and a certain number of hypotheses has to be introduced so as to supplement the lack of data; some of the main resonances (those with large elasticity) are introduced as known and the search for a solution is started from limited regions of the unitary circles. An attempt has been made, nevertheless, to

exploit these angular distributions. A very preliminary result obtained with this "mixed" method is shown in Fig. 5 from ref. 16. The features of the solution of Fig. 3 are still present but much more structure is introduced. The data being what they are, it is unlikely that anything much better than this can be extracted by similar approaches.

The situation above ~ 1 GeV/c is markedly different. The amplitudes are known to reach values of J as high as 9/2 (if we stop at 2 GeV/c) and the required measurements must be necessarily of a much higher statistical precision. It is difficult to assess what is the exact level of statistics necessary to give a meaningful measurement of a 9th order coefficient (it depends on the angular distribution itself, on the solid angle covered, etc.). The data that will be available at the completion of the current bubble chamber experiments[17,18,19] will hopefully reach the required accuracy for the differential cross sections of both $K^-p \to K^-p$ and $K^-p \to \bar{K}^0n$. The recent series of polarization measurements of $K^-p \to K^-p$ in this region[20] are already the best one can hope to make without a much larger and more expensive effort.

In conclusion, from the experimental point of view, the situation will be, at best, roughly comparable to that just described below ~ 1 GeV/c. But there will be a notable difference in complexity of the problem. To start with, the resonances are here far less important, their elasticities reaching at most ~ 20 °/o as compared to the ~ 65 °/o of the previous region; thus, for example, it will be much harder to defend such simple-minded approaches as assuming that a resonance is the "dominant feature" of a certain energy region. Second, the very large number of amplitudes (20 if $J \leq 9/2$), together with their possible permutations, will make the establishment of a "unique" solution an absolute nightmare. The

higher energy available will furthermore result in a wider variety of decay channels for the resonances present; this, in turn, will make the complementary study of their inelastic channels much harder (there will be less statistics per individual channel, proportionately less 2-body channels, etc.).

Without extending further this discouraging list of difficulties which will be encountered in the analysis of the $\bar{K}N$ interaction between 1 and 2 GeV/c, we would like to stress the point that much more information should be made available in this energy range if a definitive interpretation is to be done at all. The additional piece of information could come from any of the processes under (b) to (d) above. The easiest, we claim, is the differential cross section of $K^- n \to K^- n$.

Let us assume that this measurement is done; we can add it to the data on the differential cross sections for $K^- p \to K^- p$, $K^- p \to \bar{K}^0 n$, the polarization of $K^- p \to K^- p$ and the two isospin cross sections, σ_0 and σ_1. There are 40 unknowns (assuming $J_{max} = 9/2$) and 41 equations: the problem is still formidable, but there is some hope.

III. Use of the deuteron as a free nucleon target.

There are three major facts to consider in a $K^- n$ interaction. First, the target is not at rest: it moves with an average Fermi momentum of $\sim$ 60 MeV/c. Second, the K^- also interacts with the remaining nucleon of the deuteron: this is the Glauber (or screening) effect. Third, the scattered nucleon interacts with the other nucleon: this gives rise to a final-state interaction.

When dealing with the experimental data, the effect of the Fermi motion can be easily accounted for. The resulting spread in centre of mass energy is sometime even advantageous: the continuous energy spectrum obtained can be apportioned in the most convenient way for the purpose of the subsequent analysis.

The effect of the other two phenomena is, in principle, exactly calculable. In practice, however, some of the ingredients are just those quantities which we are looking for, i.e. the $\bar{K}N$ amplitudes. On the other hand, these can be estimated and used to tell us if the correction required is important or not. An approximate calculation is usually introduced to take into account the screening effect (see, for example, section III (2) below). The final-state interaction appears to be of negligible importance already at incident momenta of the order of 1 GeV/c.

In what follows we shall review the experimental situation concerning reactions on nucleons bound in a deuteron.

1. The pion-nucleon interaction has been thoroughly investigated by means of πp collisions (differential cross sections and polarizations of the reactions $\pi^+ p \to \pi^+ p$, $\pi^- p \to \pi^- p$, $\pi^- p \to \pi^0 n$) and is sufficiently well known to offer, in principle, an excellent basis of comparison for the case where the target nucleon is bound in a deuteron. Unfortunately, the experimental situation is not nearly as good when it comes to πd collisions.

From the existing material we present here the results of a bubble chamber experiment[21] where the following reactions were studied:

$$\pi^+ d \to \pi^+ p(n_s) \qquad (8)$$

$$\pi^+ d \to \pi^+ n(p_s) \qquad (9)$$

The criteria for defining which is the spectator particle (n_s and p_s) are based on the final state momenta and discussed in ref. 21. It is also shown that the momentum spectrum of the spectator particle is in agreement with the calculations of the deuteron wave-function. Differential cross sections have been obtained at several values of the c.m. energy and an expansion in series of cos θ (where θ is the c.m. angle of the outgoing pion with respect to the incident) was then performed. The coefficients A_n of this expansion are shown in Fig. 6 for reaction (8), and Fig. 7 for reaction (9).

On these figures are also shown the analogous coefficients for the reactions $\pi^+ p \to \pi^+ p$ and $\pi^- p \to \pi^- p$, both on stationary protons. If the selection criteria are correct, and the impulse approximation is valid, the two sets of coefficients should be identical within statistics. The latter is not overwhelming (a total of about 3,000 events for each reaction and over the whole energy range), but there is no evidence for disagreement. It should be mentioned, in passing, that this same type of comparison can and will be done in our proposed experiment when measuring the reaction $\pi^- d \to \pi^- n(p_s)$. The statistical accuracy that we can easily reach, will be more than sufficient to allow a strict comparison.

2. The total cross sections for $K^- p$ and $K^- d$ collisions have been measured very precisely by the counter experiments of refs. 3, 4 and 5 over a momentum range extending from ~ 0.6 to ~ 3.3 GeV/c. The pure isospin cross sections, σ_0 and σ_1, were extracted from the measurements in the following way. The measured cross sections can be written as

$$\sigma_{K^- p} = \frac{1}{2}\sigma_0 + \frac{1}{2}\sigma_1 \qquad (10)$$

$$\sigma_{K^- d} = \frac{1}{2}"\sigma_0" + \frac{3}{2}"\sigma_1" - \sigma_G \qquad (11)$$

where the terms between inverted commas refer to quantities spread out by the Fermi momentum. The term σ_G represents the Glauber correction

$$\sigma_G = (1/4\pi) < r^{-2} > \sigma_{K^-p} \sigma_{K^-n} \qquad (12)$$

where $< r^{-2} >$ is the average of the inverse square of the separation of the nucleons in the deuteron; the term containing the product of the real parts of the forward scattering amplitudes was neglected. The measured cross section on stationary proton, σ_{K^-p}, was then spread-out according to

$$"\sigma_{K^-p}(S)" = \int \sigma_{K^-p}(S') \mid \Psi (q)|^2 \, d^3q \qquad (13)$$

where $S = (p_1 + p_2)^2$ and $S' = (p_1 + p_2 - q)^2$, p_1 and p_2 being the four-momenta of the K^- and the proton, respectively, and q the Fermi momentum of the proton in the deuteron. The deuteron wave-function is $\Psi(q)$. Using this value of "σ_{K^-p}", equations (10) and (11) were then solved for "σ_0" and "σ_1". Finally, the Fermi momentum was unfolded (reversing the operation done in equation (13)) and σ_0 and σ_1 obtained.

The results are shown in Figs. 8, 9 and 10 and are too well known to need a discussion. From these simple and classic experiments a wealth of old and new resonances came forth. The old ones ($\Sigma(1660)$, $\Sigma(1760)$, $\Lambda(1820)$) were in excellent agreement with what was already known at the time. The new ones ($\Lambda(1690)$, $\Sigma(1910)$, $\Sigma(2030)$, $\Lambda(2100)$, $\Sigma(2250)$, $\Lambda(2350)$, $\Sigma(2450)$, $\Sigma(2600)$) are presently being studied with different techniques[17][18][19] in view of a determination of their quantum numbers. Up to now, they appear to be confirmed.

The morale is that the deuteron seems to be well described, at least as far as total cross sections are concerned, by the simple picture presented above.

3. Another reaction has been reasonably well studied and offers a very convenient test ground for our comparison. This is $\underline{K^- d \to \Lambda \pi^- (p_s)}$ and the equivalent reaction on free protons $K^- p \to \Lambda \pi^0$. The cross sections for the two reactions must be in the ratio of 2 : 1 if isospin conservation is valid. The experimental methods followed for the analysis of the two reactions are described in ref. 6 (for $K^- p \to \Lambda \pi^0$) and ref. 15 (for $K^- d \to \Lambda \pi^- (p_s)$). The calculation of the deuteron wave function, corrected for the screening effect, is in good agreement with the momentum spectrum of the spectator proton shown in Fig. 11. Only spectator momenta up to 300 MeV/c have been accepted; the possibility that the proton participates in the primary collision becomes too large beyond this momentum.

The K^- momentum region where both reactions are known extends from ~ 0.6 to ~ 2 GeV/c. The comparison of these reactions can be done at all stages: total and differential cross sections, even polarizations. Fig. 12 shows, for example, the two differential cross sections at ~ 800 MeV/c.[6][15] The measurements are based on about 200 events for each reaction. The normalizations are completely independent. Fig. 13 shows the same situation at ~ 900 MeV/c; here the $\Lambda \pi^0$ reaction is drawn as a continuous histogram, the $\Lambda \pi^-$ as separate points. Also indicated is the best fit of the $\Lambda \pi^0$ data to a Legendre polynomial expansion of the type given by equation (6). The same expansion can, of course, be done over the $\Lambda \pi^-$ data and the coefficients A_n of the two sets can be compared. This is less cumbersome than inspecting a large number of angular distributions. Figs. 14 and 15 give the coefficients in question from ~ 0.6 to ~ 1.2 GeV/c[22]. Fig. 16 gives the data from ~ 1.2 to ~ 2 GeV/c from different experiments[18][19].

No systematic deviations can be seen, the agreement being overall good. It should be pointed out that the presence of a possible final state interaction between the Λ and the spectator proton has not been considered. The fact that the need for such a correction is not felt, indicates that the effect, if present, occurs at a level which is below the statistical accuracy. This is interesting, because the Λ-nucleon interaction is not very different from the nucleon-nucleon interaction, thus suggesting that final state effects in $K^- d \to K^- n\ (p_s)$ could be equivalently unnoticeable.

4. Other reactions have been studied, such as $K^- d \to \Sigma^- \pi^0 (p_s)$ and $K^- d \to \Sigma^0 \pi^- (p_s)$. Here, however, no direct comparison is possible with an equivalent reaction on stationary nucleons. The proton reactions are $K^- p \to \Sigma^+ \pi^-$, $\Sigma^- \pi^+$, $\Sigma^0 \pi^0$ and none contains a pure isospin 1 final state. An indirect test is still possible from the results of the partial wave analyses of refs. 23 and 12. These results yield a unique prediction of the $I = 1$ $\Sigma\pi$ channel. These are shown in Fig. 17 under the form of predicted differential cross sections (the dotted lines) for the reactions[16] $K^- d \to \Sigma^- \pi^0 (p_s)$, $\Sigma^0 \pi^- (p_s)$ (added together so as to gain statistics).

The agreement is very reasonable considering the approximations involved and the considerable experimental problems associated with the identification and measurement of all the reactions used.

5. A situation which is very similar to the one described above, but worse statistically, occurs for the existing experimental information[15] on $K^- d \to K^- n (p_s)$. Here again no direct comparison can be made. The $\bar{K}N$ amplitudes of refs. 10,11,12 obtained from

$K^-p \to K^-p$ and $K^-p \to \bar{K}^0n$ can be used to predict the differential cross sections of the I = 1 reaction. The comparison is made on Fig. 4 and, for what is worth, agrees once more.

6. A final comment can be made on a class of phenomena which, although not obviously connected with the reaction we propose to study, are still relevant to the issue of whether or not a bound nucleon in the deuteron can be thought of as a free target. An example of these phenomena is the process $\bar{K}N \to \Sigma(1760) \to \Lambda(1520)\pi \to \Sigma\pi\pi$. This chain of formation and decay of resonances has been observed with K^- on free protons and on bound neutrons in the reactions

$$K^-p \to \Sigma^{\pm}\pi^{\mp}\pi^0 \qquad (14)$$

$$K^-d \to \Sigma^{\pm}\pi^{\mp}\pi^-(p_s) \qquad (15)$$

in the neighbourhood of $\sim$ 950 MeV/c[24][25].

The results are remarkably similar, down to the details of the various angular distributions: the decay of $\Sigma(1760)$ into $\Lambda(1520)$ and the successive decay of $\Lambda(1520)$ into $\Sigma\pi$. Figs. 18 and 19 show the cross sections and decay angular distributions for the reactions (14) and (15) respectively. It is unlikely that such a consistent and striking similarity could be preserved in the presence of serious perturbing phenomena not yet understood.

IV. Experimental aspects

In this section, we shall first discuss the effect of the various measurement errors in order to make precise the constraints which are imposed by the apparatus. We will give at the end some technical details concerning the magnetic spectrometer and the neutron detector, calibrations and efficiencies.

1. Kinematical reconstruction: The experimental set-up that we intend to use will allow the measurement of

(a) the momentum and the angle of the scattered K using a magnetic spectrometer,

(b) the angle of the recoil neutron interacting in the polyethylene plates of a large spark chamber.

With the exception of two windows (for the K^- and the neutron), the target will be surrounded by an anticoincidence counter in order to get rid of all inelastic channels with charged particles or pi zero. At the same time, this anticoincidence introduces an average upper limit of about 250 MeV/c on the momentum of the spectator proton for the accepted events.

Using these quantities, the kinematical reconstruction of the events amounts to the resolution of a second order equation, sometimes called a "zero-constraint" fit. We have checked, using a sample of randomly generated events, that there is no ambiguity in the choice of the good solution as long as the scattered neutron momentum is greater than ~ 300 MeV/c which is also the limit above which one can distinguish if the scattering has taken place on a neutron rather than on a proton.

The quality of the reconstruction has been estimated with a Monte Carlo method. The computation was done for a certain number of fixed scattering angles of the K meson, corresponding to various settings of the spectrometer. The momentum distribution of the target neutron inside the deuteron was generated according to the Hulthèn wave function. The events were then reconstructed taking into account the following uncertainties (a) the beam momentum spread, (b) the measurement errors affecting the scattered K^- momentum and (c) the angular errors of both the K^- and the neutron. For each event the deviations between the generated and the reconstructed centre of mass energy (E_{cms}) and the K^- scattering angle (θ_{cm}) have been calculated. The histograms of these deviations are shown on Fig. 20 and 21 for two values of the incident K^- momentum and different error sets as described in their respective figure captions.

It is interesting to study the effect of each error-source on the final resolution:

(a) the error on E_{cms} is, of course, very much dependent on the uncertainty in the incident momentum; to be able to get a resolution better than $\pm$ 0.5 °/o, the uncertainty on the incident momentum must not be larger than $\pm$ 1 °/o. Thus one could either work with a momentum bite smaller than $\pm$ 1 °/o or use a hodoscope (proportional wire-chamber) to measure each kaon in the momentum-dispersed beam - this last solution having the advantage of a higher rate of data taking.

(b) the accuracy of the momentum determination of the scattered K^-, using a magnetic spectrometer with a field of 10 KG, is of the order of $\Delta p/p = \pm 8\ 10^{-3} p(GeV/c)$ i.e. 1 to 2 °/o in the energy range considered. This has some importance only for the forward angles. Both E_{cms} and $\cos \theta_{cm}$ are insensitive to the exact value of the momentum for a backward K^- within the errors limits given above.

(c) The K^- scattering angle is obtained by measuring the incident and scattered K^- with proportional wire-chambers. The maximum uncertainty on this angle is at most 10 mrd including the multiple scattering; the contribution of this uncertainty to the resolution both in E_{cms} and $\cos_{cm}$ is minor. This is also the case for the angle of the recoil neutron: an accuracy of 20 mrd can easily be achieved, this being largely sufficient.

The reconstruction of $\cos \theta_{cm}$ is always very accurate; 98 °/o of the events are inside the range $\Delta(\cos \theta_{cm}) = \pm 0.04$. This is accurate enough for the purpose of the analyses discussed in the previous sections.

Fig. 22 shows the comparison between the input momentum distribution of the target neutron for the generated events and the same distribution after the reconstruction, again for two values of the incident momentum.

2. Angular range of the apparatus: The forward limit is due to the use of deuterium as the neutron target, as explained in the original proposal. It can be seen that it is necessary for the neutron momentum to be larger than ~ 300 MeV/c and for the spectator proton momentum to be smaller than ~ 250 MeV/c if one wants to limit to less than ~ 2 °/o the probability that the interaction has taken place on the proton rather than on the neutron. The corresponding limit on $\cos \theta_{cm}$ is given by the Fig. 6 of the original proposal.

In the very backward direction, the cms solid angle of our apparatus becomes extremely small. Moreover the decay rate of the scattered K^- decreases the efficiency of good events below a reasonable level. We have calculated an average value of - 0.85 as

the lower limit for cos θ_{cm}. Of course, this limit can be shifted if more running time is available.

Another difficulty for the very backward setting arises from the fact that, beyond cos $\theta_{cm} = -0.9$, the beam must cross the neutron detector.

3. Magnetic spectrometer: We intend to use an automatic system consisting of wire chambers working in the proportional mode. Such a system, in spite of its price, presents many advantages which are presented below.

In our measurement a correct evaluation of the absolute value of the cross section for each energy and angular interval is essential. The apparatus must therefore be fully efficient for the whole solid angle in presence of a possibly large and non-uniform background (as anticipated on the basis of our experience with the m_7 beam). The counting losses due to the dead-time of the system must also be accurately known. We think that the proportional wire-chamber offers greater security in this respect. There is no correlation between the different wires; thus the efficiency to detect more than one track is complete for the whole surface of the chamber. In addition, spurious tracks are accepted only during a period of 50 ns in contrast to the usual 300 ns for a conventional spark-chamber.

Concerning the dead-time, one can make the following estimate. When one wire is excited, its associated electronics is closed during about 500 ns. To get a counting loss of 1 %, a wire would need to be hit by $5\ 10^3$ particles in a burst of 250 ms. This number is much larger than the possible background for an individual wire in any chamber of the spectrometer. The overall efficiency will then be very high.

Another quality of the proportional wire-chamber is to deliver a fast signal which can be used directly by standard fast electronics. The frequency of occurence of the good K^-n elastic events is rather low. An automatic system will thus easily permit the simultaneous recording of data on the reaction $K^-d \rightarrow K^-p\ (n_s)$ (which is very useful to check the validity of the use of deuterium as a free nucleon target by comparison with the same reaction on free protons), and also data on the elastic scattering $K^-d \rightarrow K^-d$. For each setting of the spectrometer, we will also want to record data on the reaction $\pi^-d \rightarrow \pi^-n\ (p_s)$ and $\pi^-p\ (n_s)$ so as to have a permanent calibration of the efficiency of the neutron detector (see below in section 4). This can be done simultaneously during the K^- data taking, or in separate runs, depending on the degree of saturation of the system.

4. Neutron detector : This will consist of a series of 20 spark-chamber modules, each consisting of three polyethylene plates 1 cm thick. The system is to be triggered each time a scattered K^- is detected without accompanying charged particles.

For neutron kinetic energies below 100 MeV, the efficiency of such a device can be deduced from the measurements reported in ref. 26 with a similar device. A minimum range of two sparks has been imposed for the acceptance of a track. For higher energies, one can assume that all inelastic n C interactions will be visible. The nC diffraction elastic scattering does not contribute to the number of visible events ; its only effect is to decrease slightly the spatial resolution of the chamber. The detection rate of the system has been computed at high energy using the known nC absorption cross section and the np total cross section.

Fig. 22 gives an idea of the expected variation of the neutron detection efficiency with energy, in our spark chamber. Thinner polyethylene plates may be advantageous when working at lower energy; we will test this possibility during the calibration run. From fig. 22 one can also appreciate the contribution coming from the visible elastic np scatterings. Taking into account the range of the recoil proton inside the chamber, one can estimate that, below 500 MeV/c, about 30 $^{o}/o$ of the events will come from elastic np scatterings. For this sample a supplementary constraint can be used in the kinematical reconstruction; also a rough idea of the polarization of the scattered neutron can be deduced from these events.

A calibration of the neutron detector is needed. The best way to produce monoenergetic neutrons, starting from a convential neutron beam, is to use the neutrons scattered from a hydrogen target: a telescope measuring the angle and range of the recoiling proton can be used to monitor the number of neutrons at a fixed energy.

A permanent check on the stability of the detecting power of the chamber, will be made during the experiment by recording from time to time (or simultaneously) data from the reaction $\pi^- d \rightarrow \pi^- n\ (p_s)$. This reaction can also be used for the setting-up of the whole apparatus before using it in a K^- meson beam.

References

(1) R. Levi-Setti; Rapporteur's Talk on Strange Baryon Resonances at the 1969 Lund Conference.

(2) See, for example, R.D. Tripp; Baryon Resonances in Proc. Int. School of Physics, Varenna 1964 (Academic Press, New York) and CERN report 65-7 (Rev.).

(3) R.L. Cool et al., Phys. Rev. Letters 16 (1966) 1228.

(4) R.J. Abrams et al., Phys. Rev. Letters 19 (1967) 678.

(5) D.V. Bugg et al., Phys. Rev. 168 (1968) 1466.

(6) R. Armenteros et al., Nucl. Phys. B8 (1968) 233, for the data between ~ 800 and ~ 1200 MeV/c .

(7) R. Armenteros et al., The $\bar{K}N$ interaction from 450 to 800 MeV/c: K^-p cross sections, to be published;

(8) A. Barbaro-Galtieri et al., report presented at the 1969 Lund Conference, for the data between ~ 300 and ~ 450 MeV/c;

(9) M. Sakitt et al., Phys. Rev. 139 (1965) B719 and J.K. Kim, Phys. Rev. Letters 14 (1965) 29, for the data below ~ 300 MeV/c.

(10) R. Armenteros et al., Nuclear Phys. B3 (1967) 592, for the analysis of the $\bar{K}N$ channel, from ~ 800 to ~ 1200 MeV/c;

(11) R. Armenteros et al., Nuclear Phys. B8 (1968) 195, for the analysis between ~ 600 and ~ 800 MeV/c;

(12) R. Armenteros et al., New experimental results on the reactions $K^-p \to \bar{K}N$, $K^-p \to \Sigma\pi$ and a partial wave analysis between 430 and 800 MeV/c, internal report CERN/D.Ph.II/PHYS 69-13 (to be published), presented at the 1969 Lund Conference, for the analysis between ~ 450 and 600 MeV/c.

(13) A. Barbaro-Galtieri et al., report presented at the 1969 Lund Conference.

(14) J.K. Kim, Phys. Rev. Letters 19 (1967) 1074.

(15) R. Armenteros et al., The $\bar{K}N$ interaction from 800 to 1200 MeV/c: K^-d cross sections.

(16) R. Armenteros et al., Energy-independent partial wave analysis of the $\bar{K}N$ channel, presented at the 1969 Lund Conference.

(17) The CERN-Heidelberg Collaboration, for K^-p collisions between 1.4 and 1.8 GeV/c.

(18) The Collège de France-Rutherford Laboratory-Saclay Collaboration, for K^-p collisions between 1.2 and 1.8 GeV/c.

(19) The Birmingham-Edinburgh-Glasgow-Imperial College Collaboration, for K^-d collisions at 1.44 and 1.64 GeV/c.

(20) C. Daum et al., Nuclear Phys. B6 (1968) 273 and B7 (1969) 19.

(21) E. Pauli et al., report LPCHE-64-10, Saclay (1964).

(22) R. Armenteros et al., Nuclear Phys. B8 (1968) 183.

(23) R. Armenteros et al., Phys. Letters 24B (1967) 198; Nuclear Phys. B8 (1968) 223.

(24) R. Armenteros et al., Phys. Letters 19 (1965) 338.

(25) R.B. Bell et al., Phys. Rev. Letters 16 (1966) 203.

(26) L.G. Pondrom et al., University of Wisconsin preprint PPAR 6 (1969).

Figure captions

Fig. 1 The four established baryon octets.

Fig. 2 Measured and predicted coefficients of the Legendre polynomial expansion of eq. (6) for the reactions $K^-p \to K^-p$ and $K^-p \to \bar{K}^0n$ from ref. (12).

Fig. 3 Argand diagrams of the partial wave amplitudes in the $\bar{K}N$ channel from threshold to 1200 MeV/c : a) isospin 1 amplitudes; b) isospin 0 amplitudes - From the work of ref. (12).

Fig. 4 Differential cross sections ($d\sigma/d\cos\theta$) of the reaction $K^-n \to K^-n$ from ref. (15).

Fig. 5 Argand diagrams of the partial wave amplitudes in the K^-n channel obtained from a "mixed" approach as described in the text. From ref. (16)

Fig. 6 Coefficients of the expansion $d\sigma/d\Omega = \sum_n A_n \cos^n\theta$ for the reactions $\pi^+p \to \pi^+p$ and $\pi^+d \to \pi^+p(n_s)$ from ref. (21)

Fig. 7 Coefficients of the expansion $d\sigma/d\Omega = \Sigma A_n \cos^n\theta$ for the reactions $\pi^-p \to \pi^-p$ and $\pi^+d \to \pi^+n(p_s)$ from ref. (21).

Fig. 8 Total K^-N cross sections for isospin 0 and 1 from ref. (3).

Fig. 9 Total K^-N cross sections for isospin 0 and 1 from ref. (4).

Fig. 10 Total K^-N cross sections for isospin 0 and 1 from ref. (5)

Fig. 11 Momentum distribution of the spectator proton in the reaction $K^-d \to \Lambda\pi^-(p_s)$ from ref. (15).

Fig. 12 The differential cross sections ($d\sigma/d\cos\theta$) for the reactions $K^-p \to \Lambda\pi^0$ and $K^-d \to \Lambda\pi^-(p_s)$ at 806 MeV/c from refs. (6) and (15).

Fig. 13 Same as in fig. 12 but at 904 MeV/c.

Fig. 14 A_n coefficients of eq. (6) for the reactions $K^-p \to \Lambda\pi^0$ and $K^-n \to \Lambda\pi^-$ from ref. (22).

Fig. 15 B_n coefficients of eq. (7) for the reactions $K^-p \to \Lambda\pi^0$ and $K^-n \to \Lambda\pi^-$ from ref. (22).

Fig. 16 A_n coefficients of eq. (6) for the reactions $K^-p \to \Lambda\pi^0$ and $K^-n \to \Lambda\pi^-$ from refs. (18) and (19).

Fig. 17 Differential cross sections for the reactions $K^- n \to \Sigma^- \pi^0$ and $\Sigma^0 \pi^-$ (added together) and the predicted distribution from the I = 1 components of the partial wave amplitudes solution of ref. (23).

Fig. 18 $\Sigma(1760) \to \Lambda(1520) + \pi$ (on hydrogen) from ref. (24).

Fig. 19 $\Sigma(1760) \to \Lambda(1520) + \pi$ (on deuterium) from ref. (25).

Fig. 20 Resolution of cms energy and cos θ_{cm} as calculated by a Monte Carlo method for different values of the laboratory angle of the scattered K^- in $K^- d \to K^- n$ (p_s). The following uncertainties have been assumed :

- incident K^- momentum : $\Delta p/p = \pm 1$ %
- scattered K^- momentum : $\Delta p/p = \pm 1$ %
- scattered K^- angle : $\Delta\theta_K = \pm 10$ mr
- neutron recoil angle : $\Delta\theta_n = \pm 20$ mr

The hatched histograms correspond to an incident momentum of 2 GeV/c; the other to an incident momentum of 1.2 GeV/c.

Fig. 21 Same as in fig. 20 but with the $\Delta p/p$ of both the incident and scattered K^- momentum equal to ± 2 %.

Fig. 22 Comparison between the momentum distribution of the neutron target inside the deuteron (Hulthèn wave-function) and the same distribution after reconstruction, using the error set listed in the figure caption of fig. 20. The continuous curve corresponds to the Hulthèn function ; the hatched histogram to the results of the Monte Carlo calculation at 2 GeV/c; the other, to the calculation at 1.2 GeV/c.

Fig. 23 Efficiency of a neutron detector consisting of 60 polyethylene plates 1 cm thick. The hatched part shows an estimate of the visible neutron interactions expected when requiring at least two sparks to define an interaction. The contribution of the np elastic scatterings is also shown.

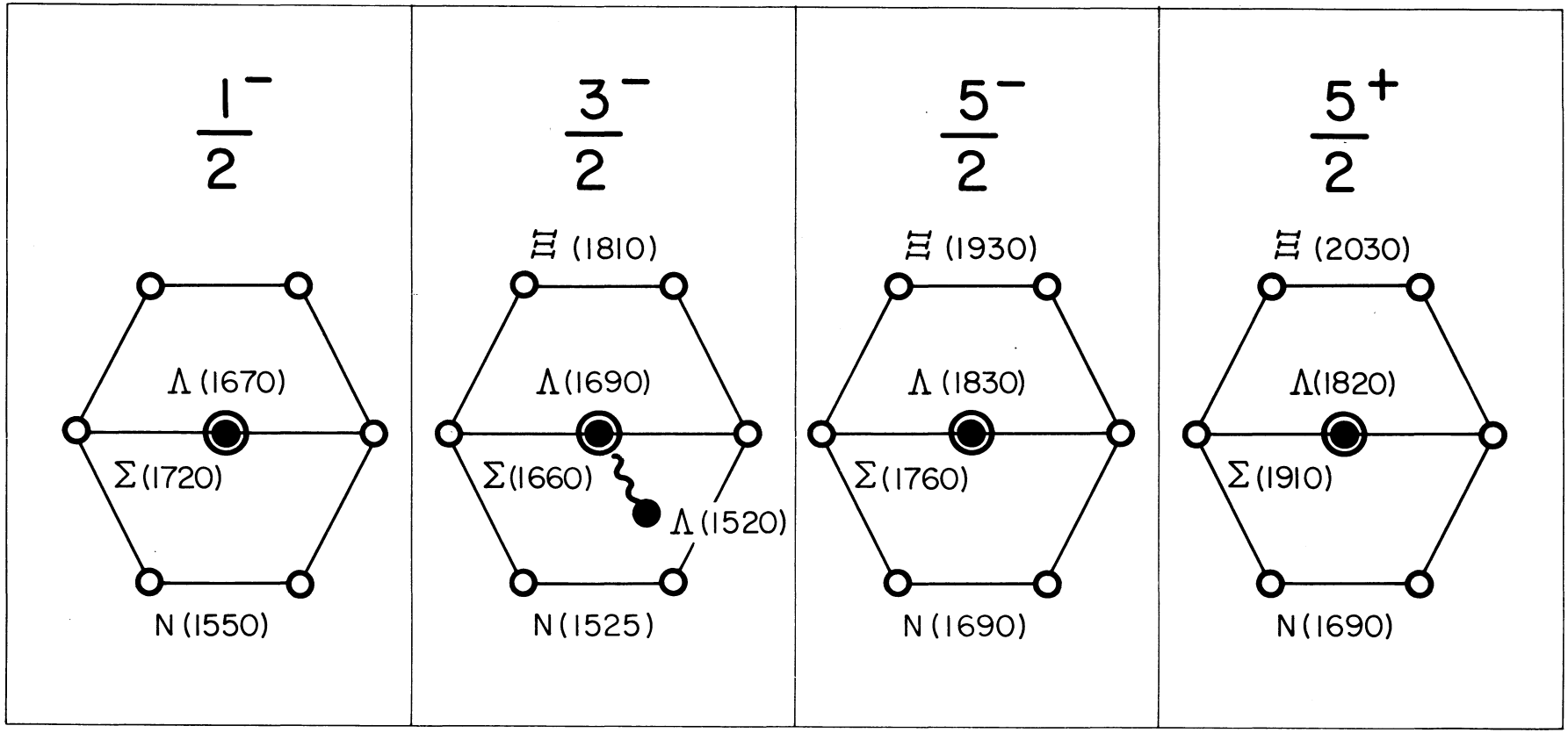
1/2⁻
Λ (1670)
Σ(1720)
N (1550)
3/2⁻
Ξ (1810)
Λ(1690)
Σ(1660)
Λ (1520)
N(1525)
5/2⁻
Ξ (1930)
Λ (1830)
Σ(1760)
N (1690)
5/2⁺
Ξ (2030)
Λ(1820)
Σ (1910)
N (1690)

FIG. 1

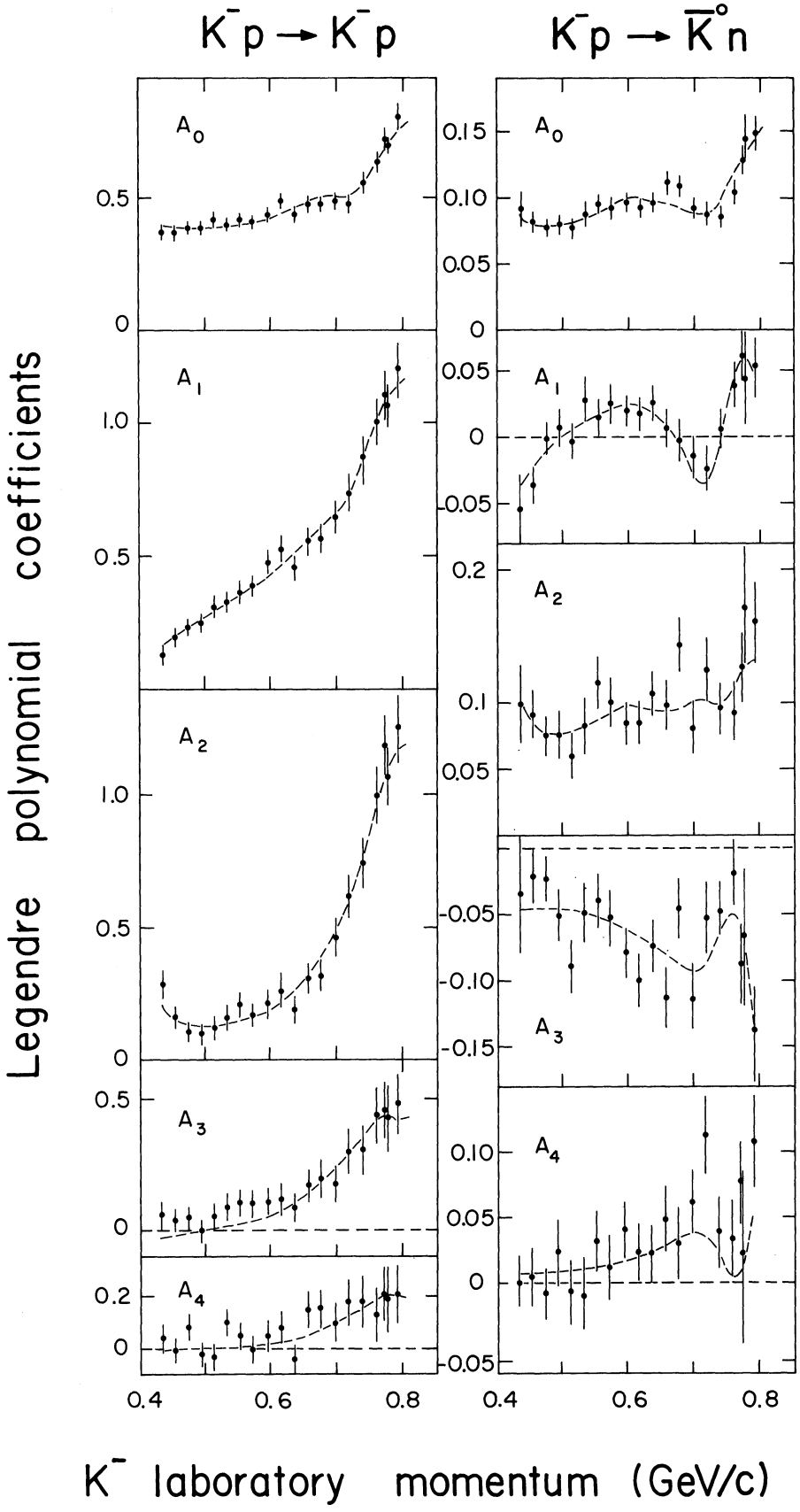
$K^-p \rightarrow K^-p$
$K^-p \rightarrow \bar{K}^0n$
Legendre polynomial coefficients
A_0
A_1
A_2
A_3
A_4
0.5
0
1.0
0.15
0.10
0.05
-0.05
0.2
0.1
-0.10
-0.15
0.4
0.6
0.8
K^- laboratory momentum (GeV/c)

FIG. 2

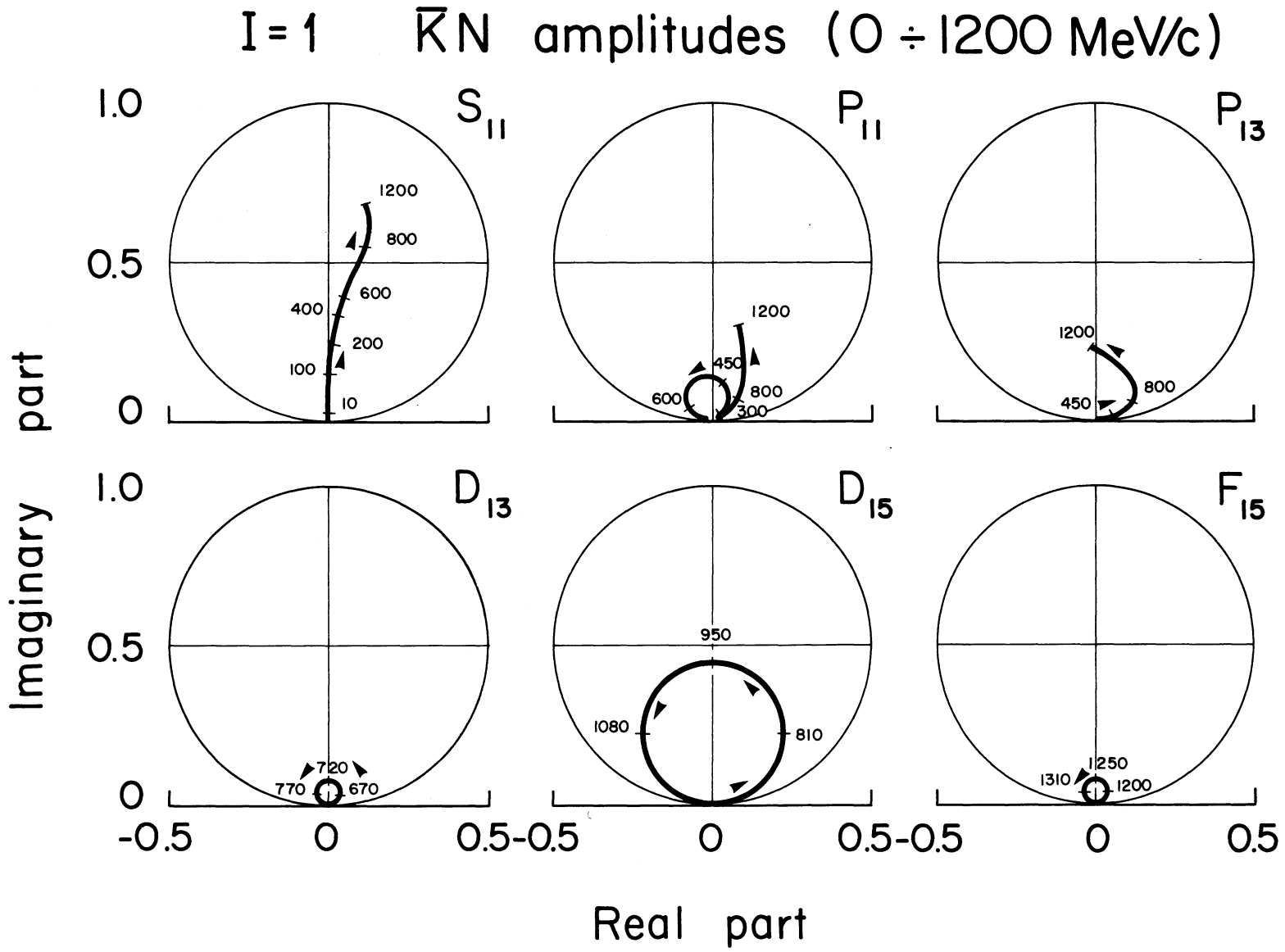
I = 1 $\bar{K}N$ amplitudes (0 ÷ 1200 MeV/c)
S_{11}
P_{11}
P_{13}
D_{13}
D_{15}
F_{15}
1.0
0.5
0
-0.5
0
0.5
1200
800
600
400
200
100
10
450
300
720
770
670
950
1080
810
1250
1310
Imaginary part
Real part

FIG. 3a

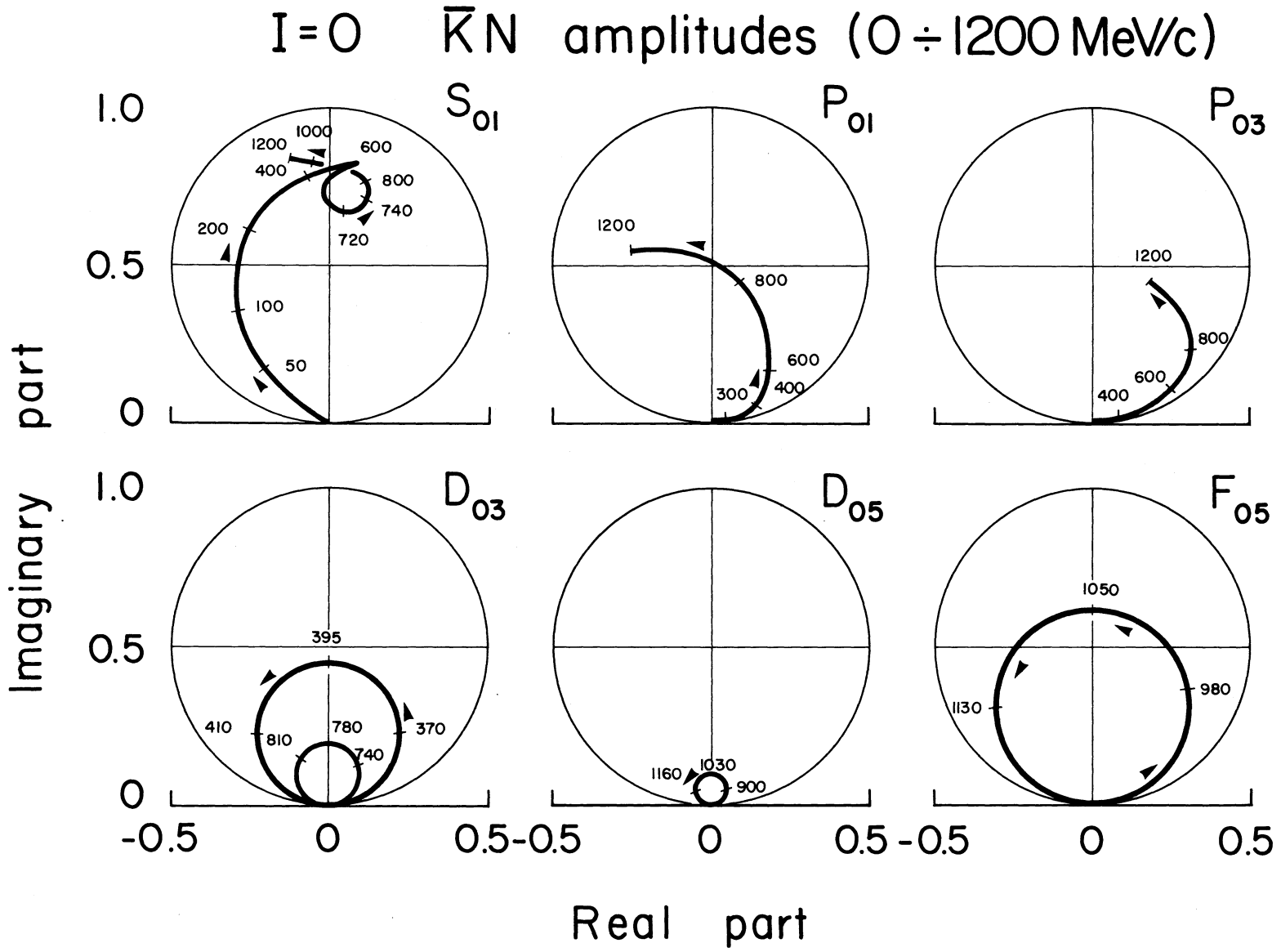
I=0 $\bar{K}N$ amplitudes (0÷1200 MeV/c)
S_{01}
P_{01}
P_{03}
D_{03}
D_{05}
F_{05}
1.0
0.5
0
-0.5
0
0.5
Imaginary part
Real part
1000
1200
600
400
800
740
720
200
100
50
1200
800
600
300
400
1200
800
600
400
395
410
810
780
740
370
1160
1030
900
1050
1130
980

FIG. 3b

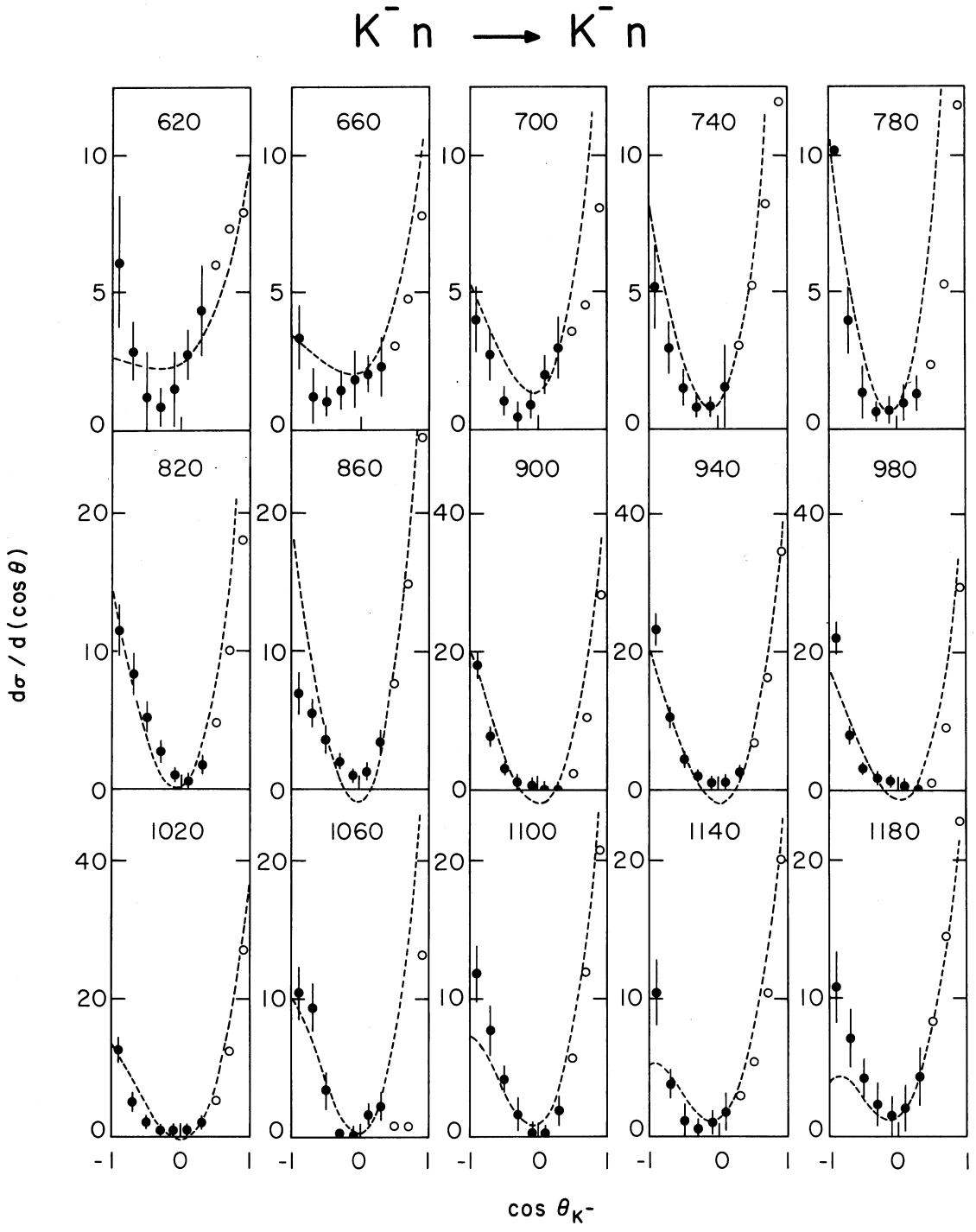
K⁻n → K⁻n
620
660
700
740
780
820
860
900
940
980
1020
1060
1100
1140
1180
dσ / d (cos θ)
cos θK⁻

FIG. 4

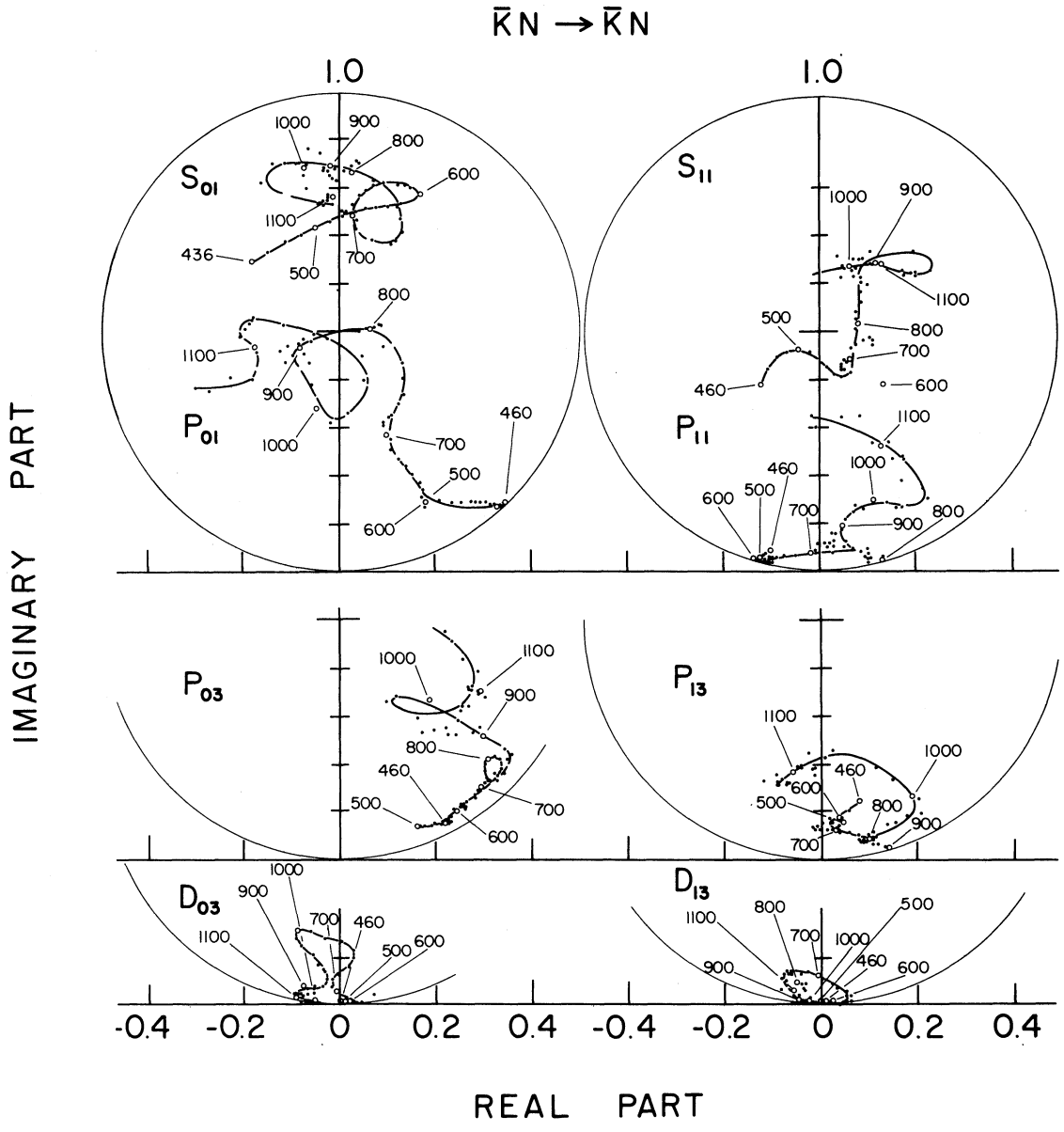
$\bar{K}N \rightarrow \bar{K}N$
1.0
1.0
S_{01}
P_{01}
S_{11}
P_{11}
P_{03}
P_{13}
D_{03}
D_{13}
IMAGINARY PART
REAL PART
-0.4
-0.2
0
0.2
0.4

FIG. 5

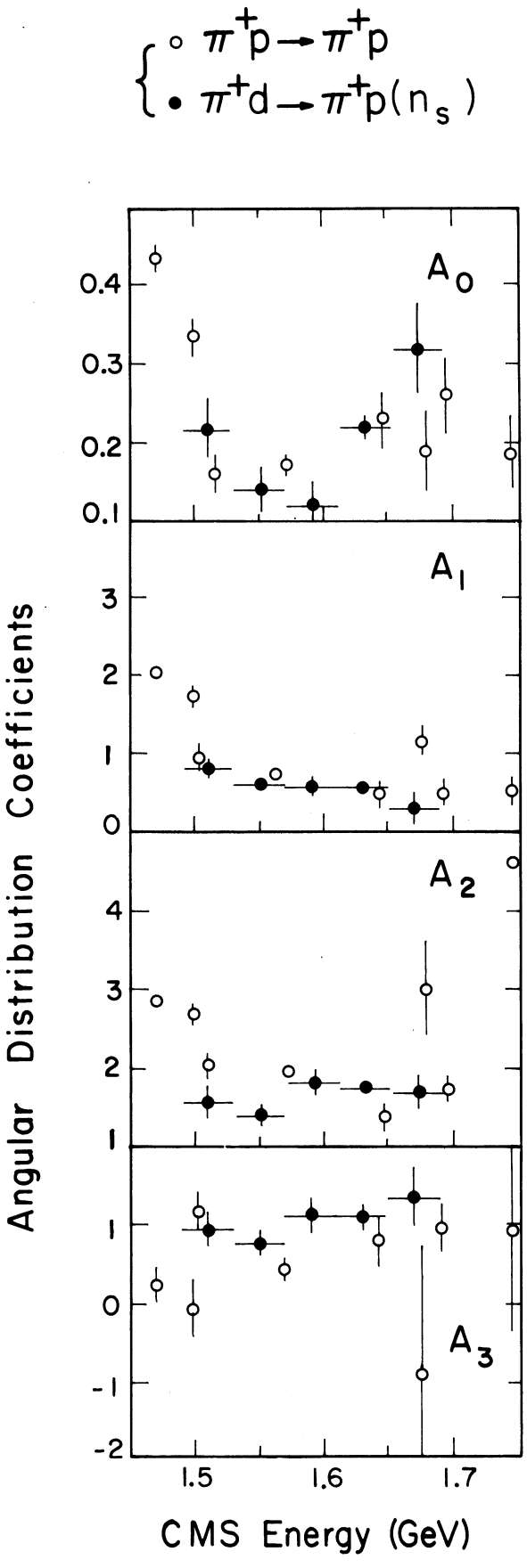
○ $\pi^+ p \rightarrow \pi^+ p$
● $\pi^+ d \rightarrow \pi^+ p(n_s)$
A_0
A_1
A_2
A_3
0.4
0.3
0.2
0.1
3
2
1
0
4
3
2
1
1
0
-1
-2
1.5
1.6
1.7
Angular Distribution Coefficients
CMS Energy (GeV)

FIG. 6

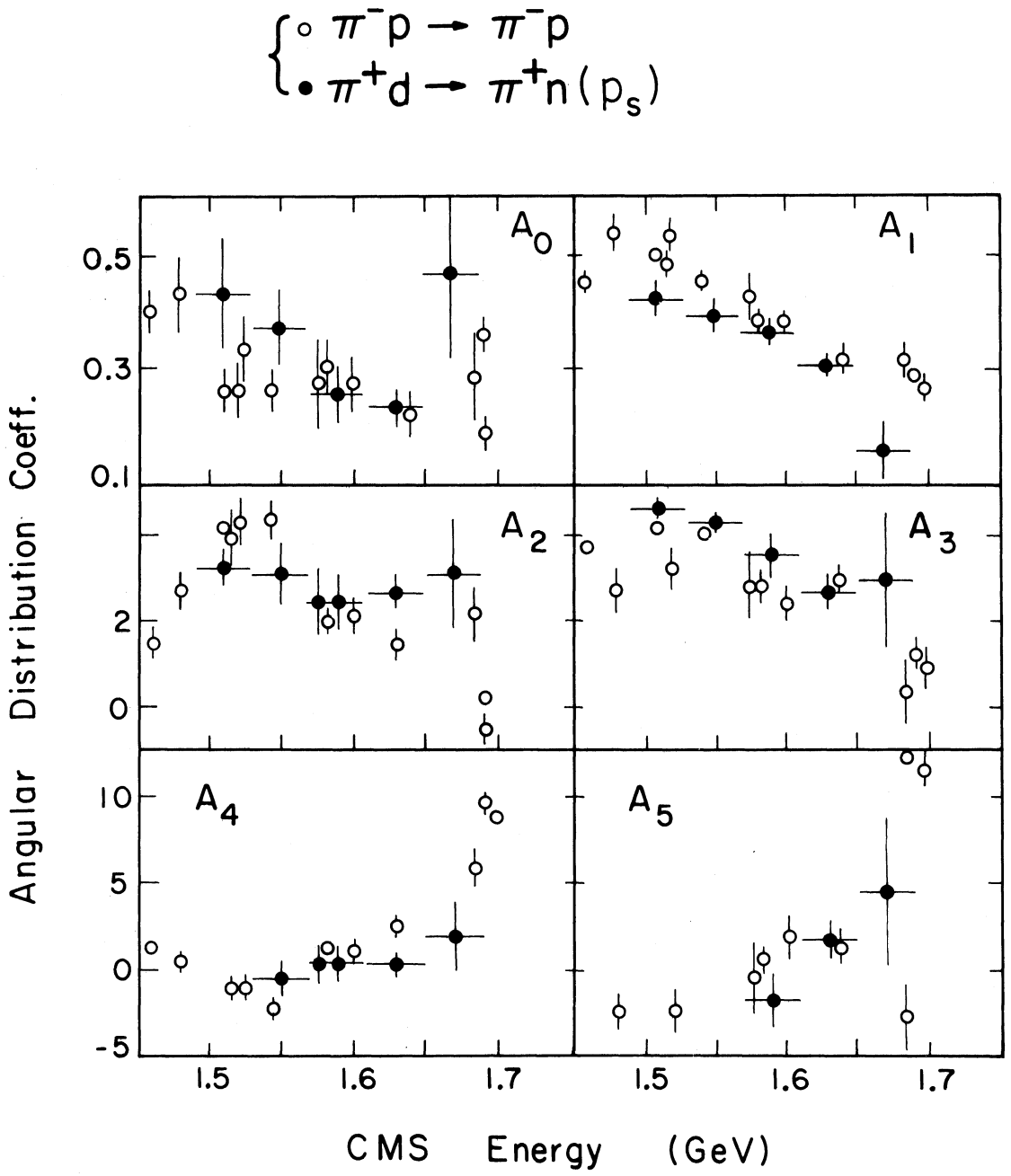
$\circ\ \pi^- p \rightarrow \pi^- p$
$\bullet\ \pi^+ d \rightarrow \pi^+ n(p_s)$
A_0
A_1
A_2
A_3
A_4
A_5
0.5
0.3
0.1
2
0
10
5
0
-5
1.5
1.6
1.7
Angular Distribution Coeff.
CMS Energy (GeV)

FIG. 7

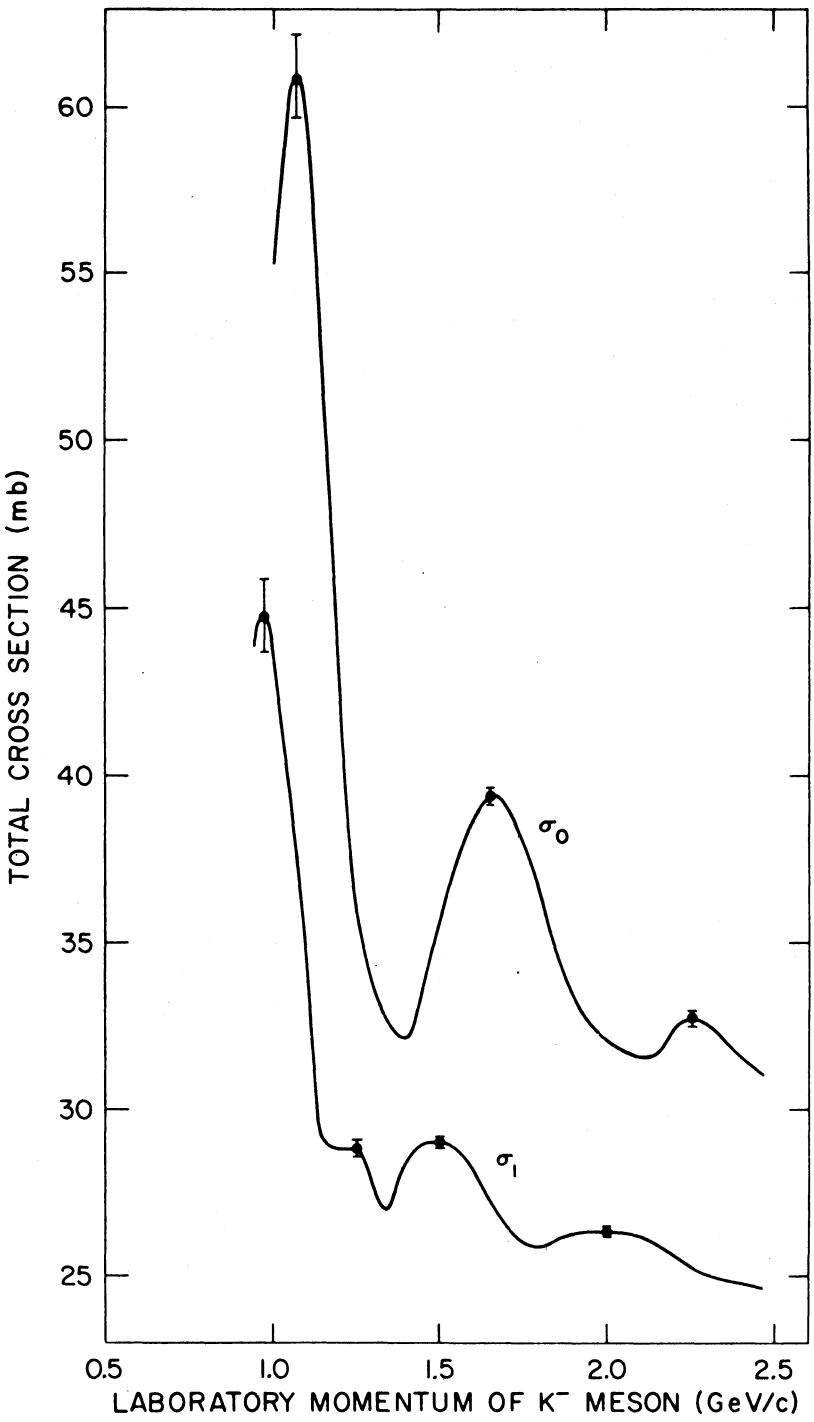

FIG. 2. The total cross sections σ_0 and σ_1 for the $I=0$ and $I=1$ isotopic spin states, respectively, for the K^-N system; typical statistical errors for a single point are shown for each structure.

FIG 8

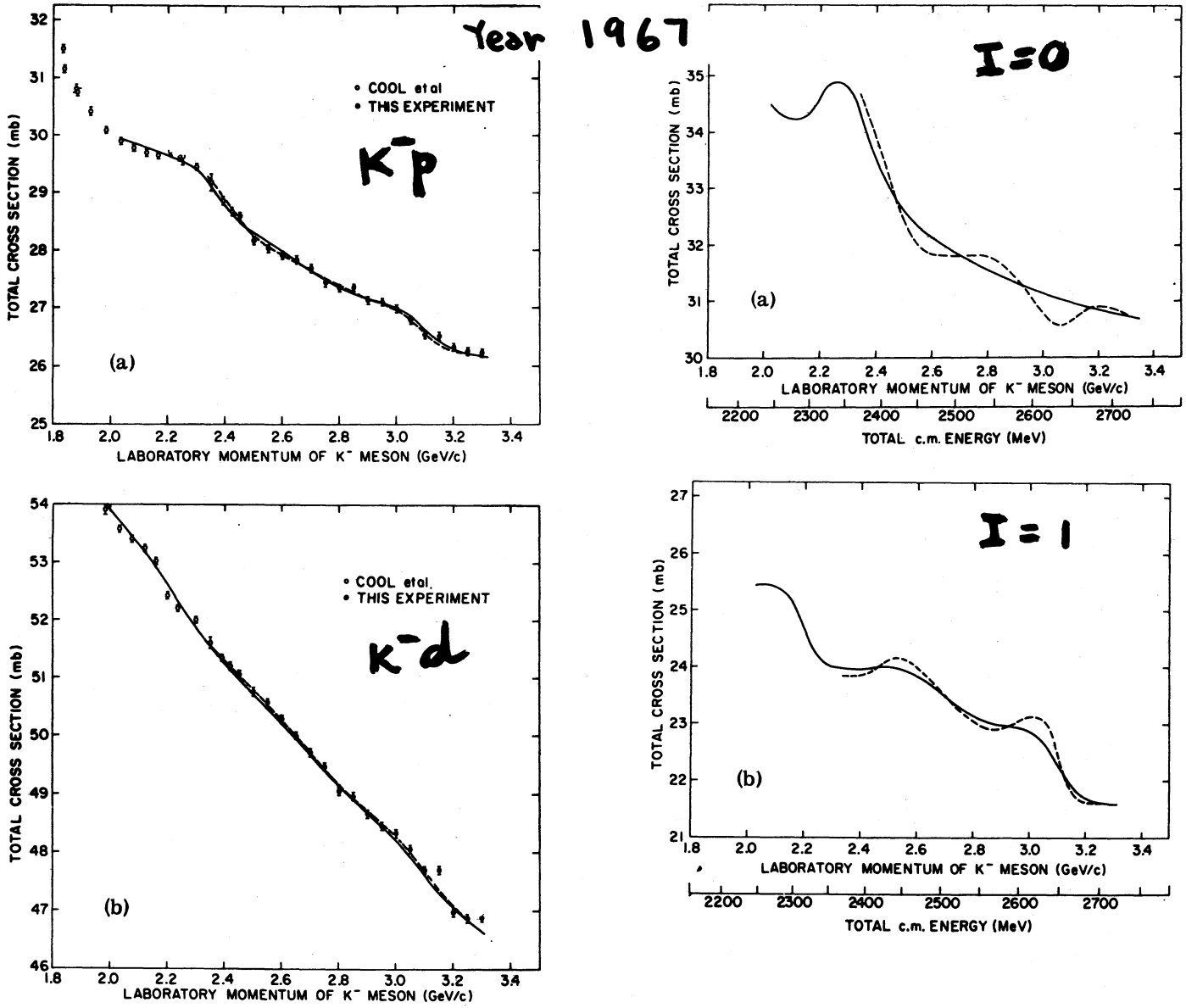
Year 1967
• COOL et al
• THIS EXPERIMENT
K⁻p
(a)
TOTAL CROSS SECTION (mb)
LABORATORY MOMENTUM OF K⁻ MESON (GeV/c)
I=0
TOTAL c.m. ENERGY (MeV)
• COOL et al.
• THIS EXPERIMENT
K⁻d
(b)
I=1

FIG 9

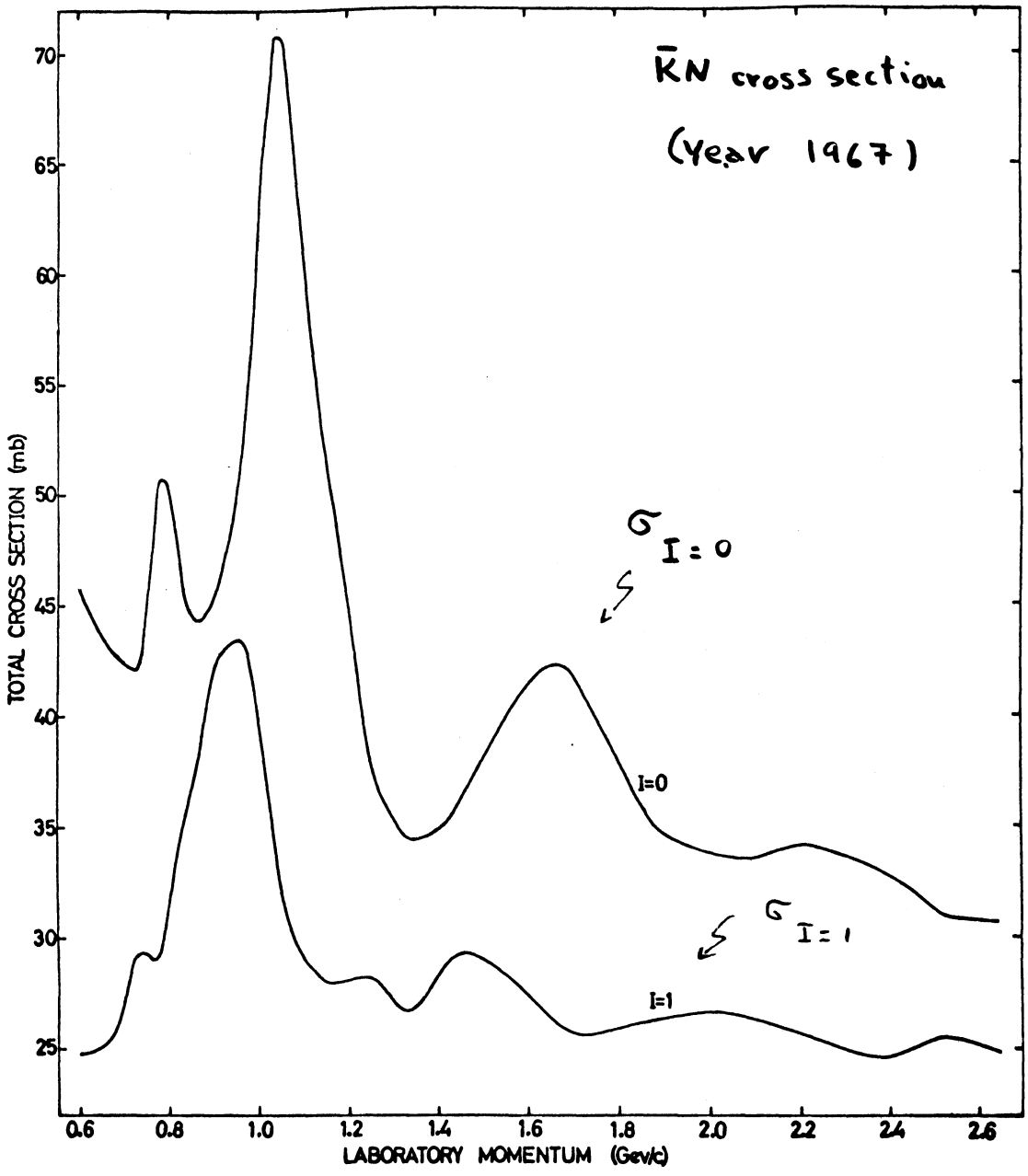
$\bar{K}N$ cross section
(Year 1967)
$\sigma_{I=0}$
$\sigma_{I=1}$
I=0
I=1
TOTAL CROSS SECTION (mb)
LABORATORY MOMENTUM (Gev/c)
70
65
60
55
50
45
40
35
30
25
0.6
0.8
1.0
1.2
1.4
1.6
1.8
2.0
2.2
2.4
2.6

FIG. 10

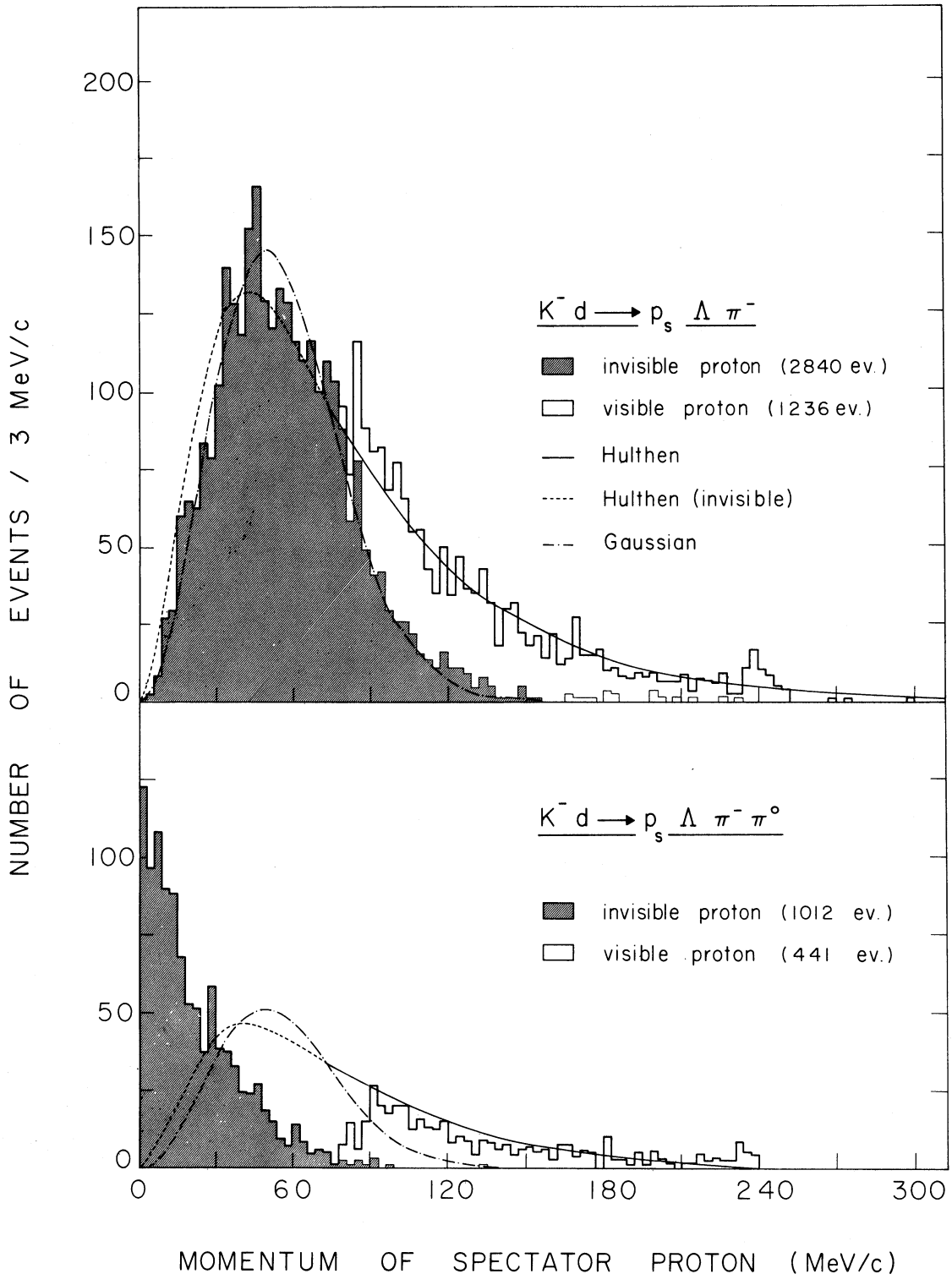
200
150
100
50
0
$K^- d \longrightarrow p_s \Lambda \pi^-$
invisible proton (2840 ev.)
visible proton (1236 ev.)
Hulthen
Hulthen (invisible)
Gaussian
100
50
0
$K^- d \longrightarrow p_s \Lambda \pi^- \pi^\circ$
invisible proton (1012 ev.)
visible proton (441 ev.)
0
60
120
180
240
300
NUMBER OF EVENTS / 3 MeV/c
MOMENTUM OF SPECTATOR PROTON (MeV/c)

FIG. 11

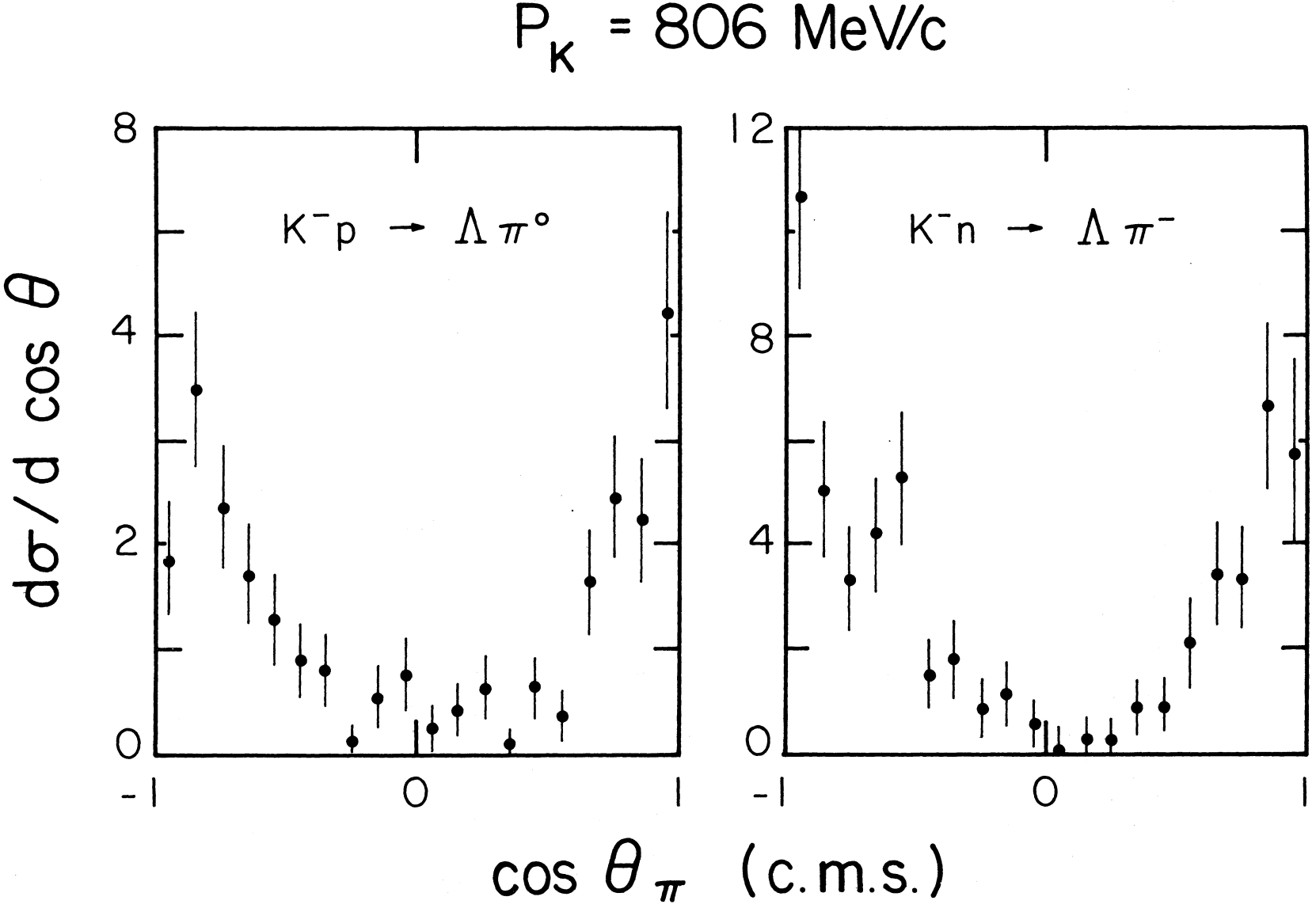
P_K = 806 MeV/c
$K^-p \rightarrow \Lambda\pi^\circ$
$K^-n \rightarrow \Lambda\pi^-$
$d\sigma/d\cos\theta$
$\cos\theta_\pi$ (c.m.s.)
8
4
2
0
12
8
4
0
-1
0
1

FIG. 12

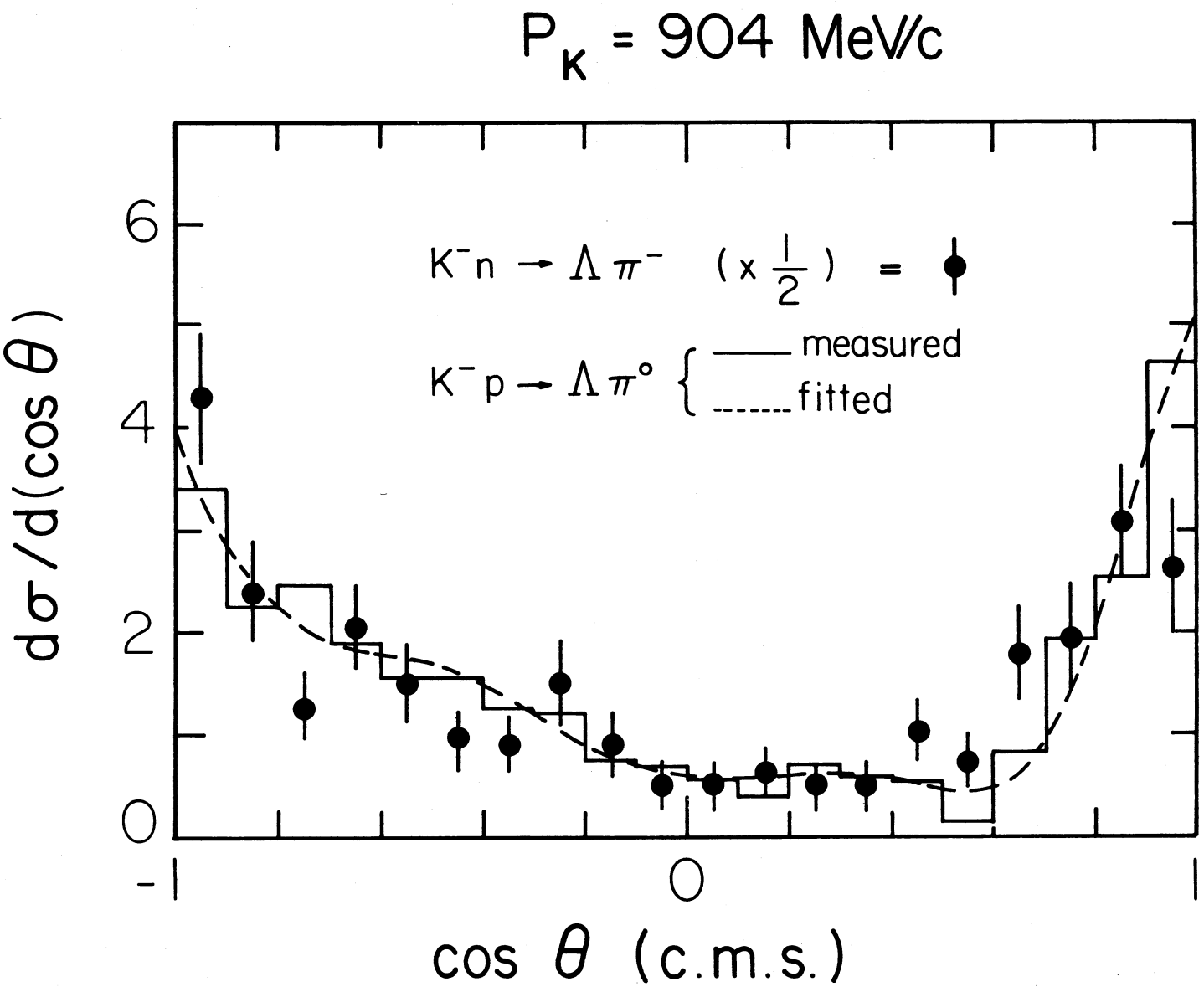
P_K = 904 MeV/c
$K^- n \rightarrow \Lambda \pi^-$ ($\times \frac{1}{2}$) =
$K^- p \rightarrow \Lambda \pi^\circ$
measured
fitted
$d\sigma/d(\cos\theta)$
6
4
2
0
-1
0
1
cos θ (c.m.s.)

FIG. 13

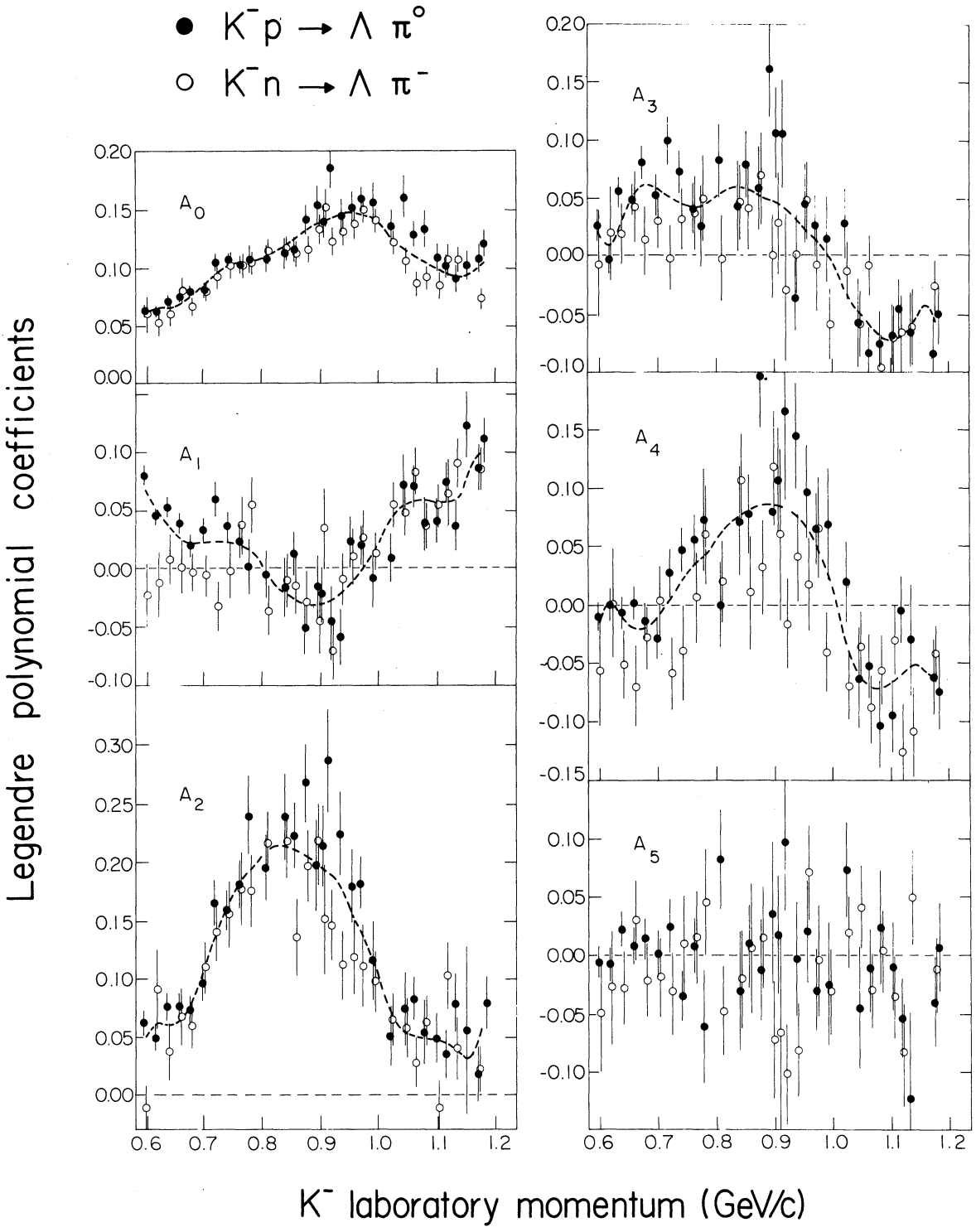
● K⁻p → Λ π°
○ K⁻n → Λ π⁻
A0
A1
A2
A3
A4
A5
Legendre polynomial coefficients
K⁻ laboratory momentum (GeV/c)

FIG. 14

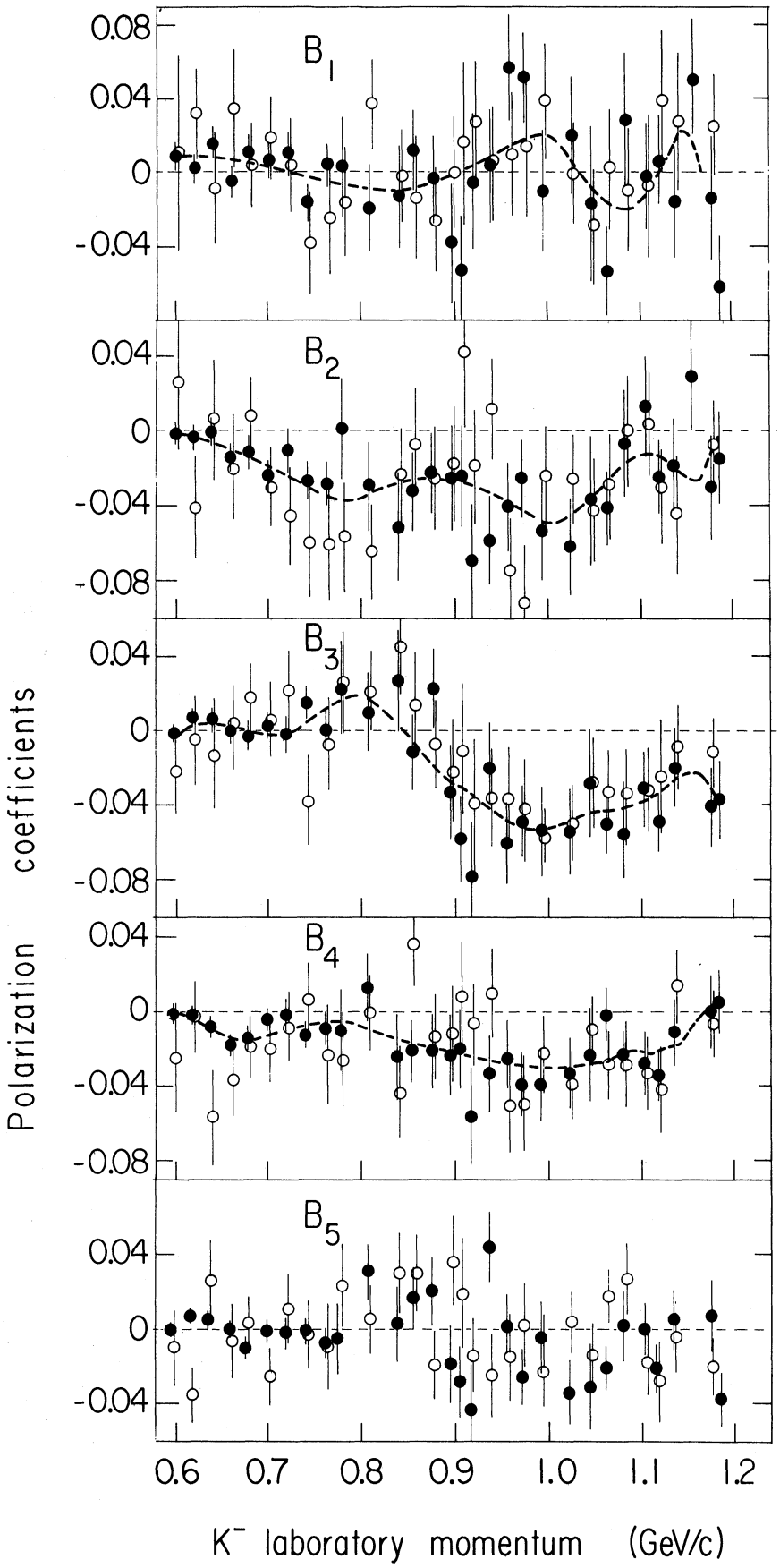
B1
B2
B3
B4
B5
0.08
0.04
0
-0.04
-0.08
Polarization coefficients
0.6
0.7
0.8
0.9
1.0
1.1
1.2
K⁻ laboratory momentum (GeV/c)

FIG. 15

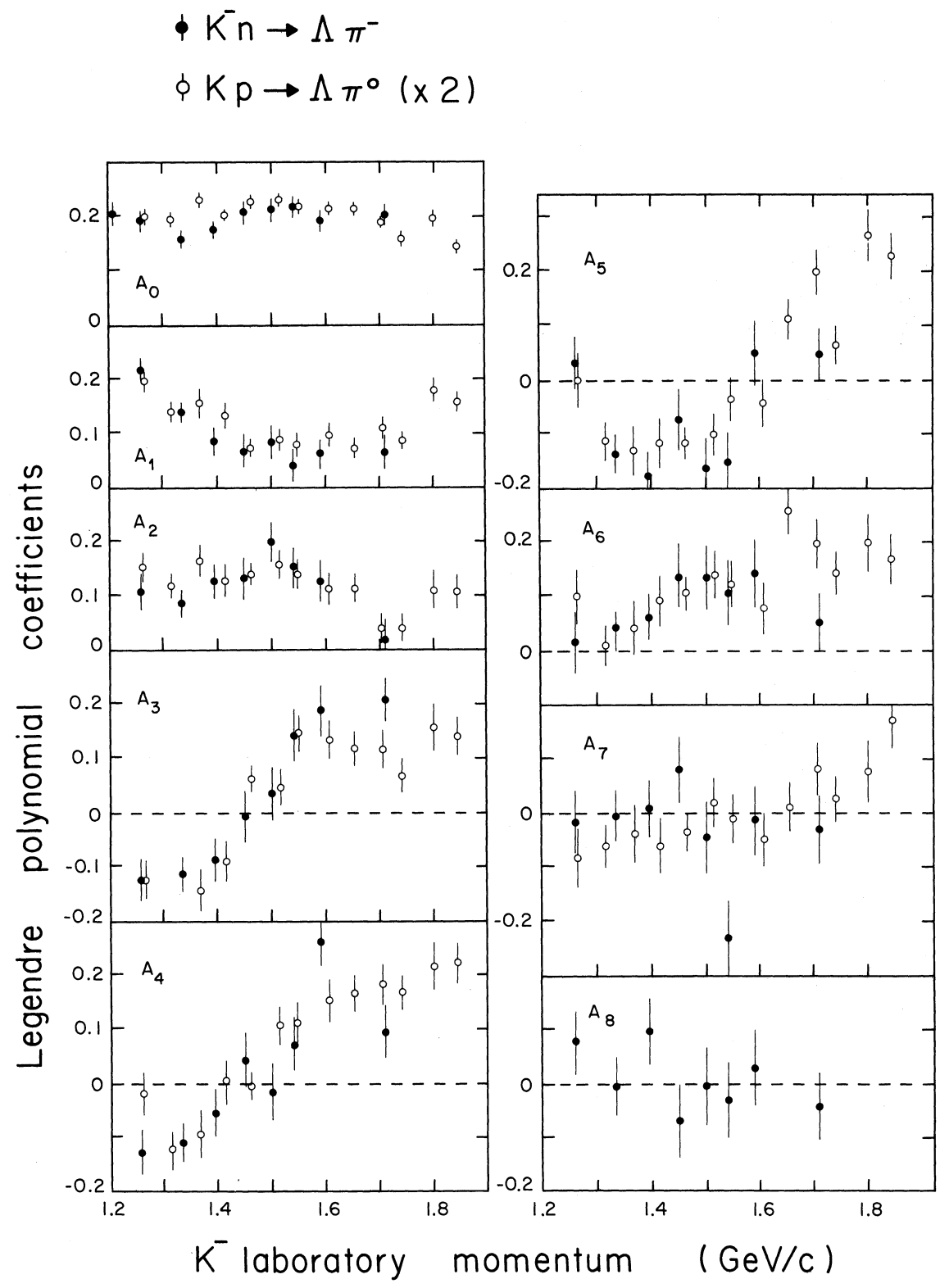
$K^-n \rightarrow \Lambda\pi^-$
$Kp \rightarrow \Lambda\pi^\circ$ (x 2)
Legendre polynomial coefficients
A_0
A_1
A_2
A_3
A_4
A_5
A_6
A_7
A_8
0.2
0.1
0
-0.1
-0.2
1.2
1.4
1.6
1.8
K^- laboratory momentum (GeV/c)

FIG. 16

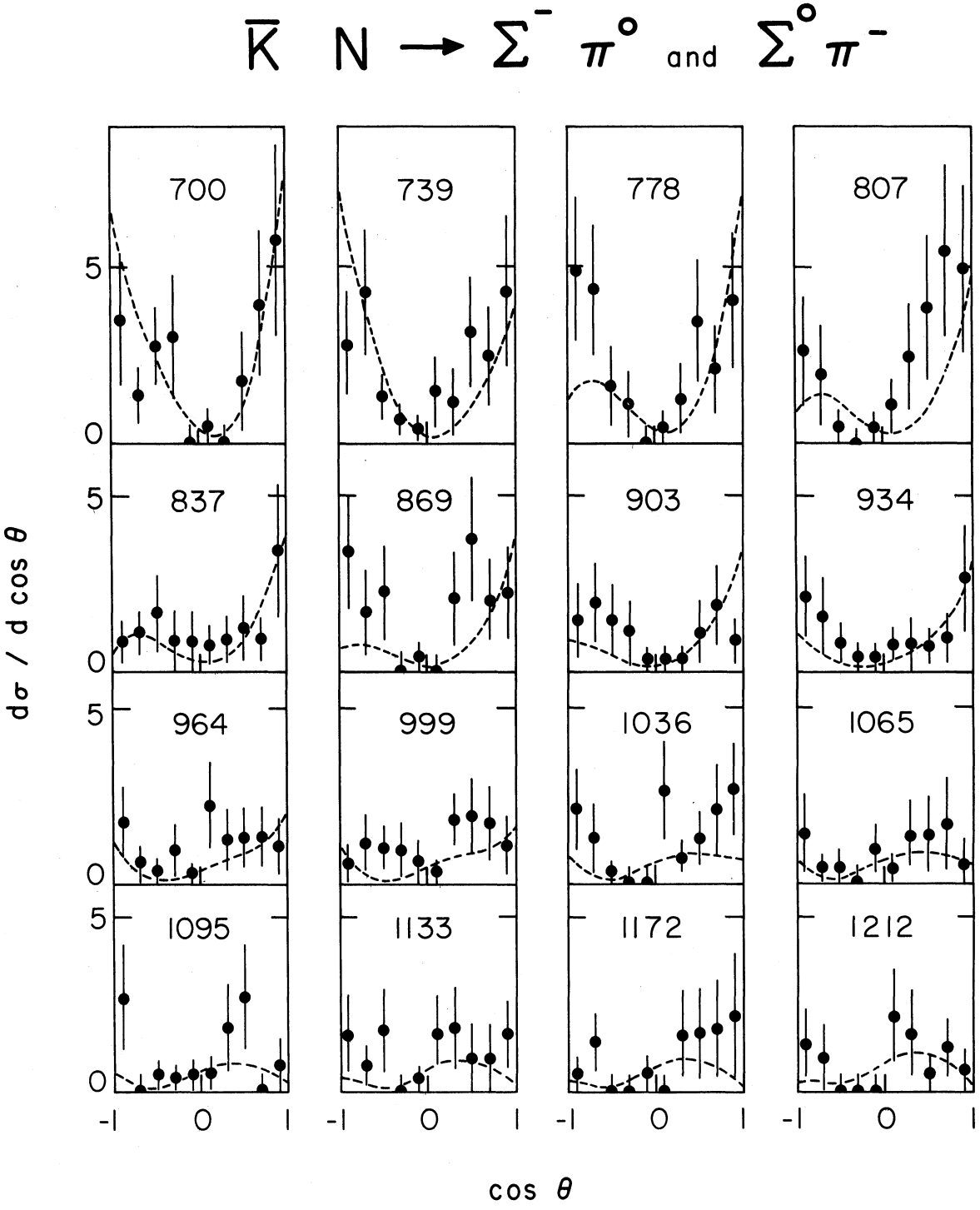
$\bar{K}\ N \rightarrow \Sigma^-\ \pi^\circ$ and $\Sigma^\circ\ \pi^-$
700
739
778
807
837
869
903
934
964
999
1036
1065
1095
1133
1172
1212
5
0
-1
0
1
$d\sigma$ / d cos θ
cos θ

FIG. 17

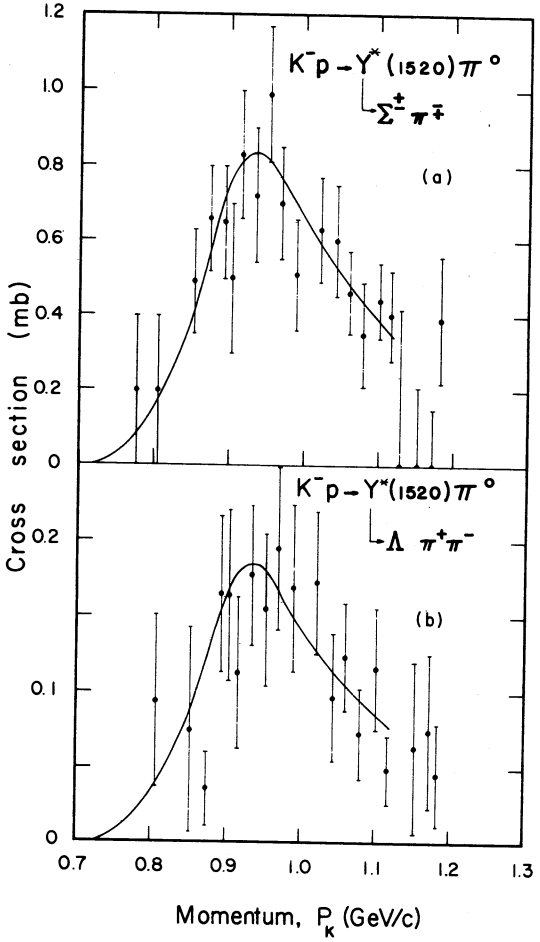
$K^-p \to Y^*(1520)\pi^0$
$\to \Sigma^\pm \pi^\mp$
(a)
$K^-p \to Y^*(1520)\pi^0$
$\to \Lambda\ \pi^+\pi^-$
(b)
Cross section (mb)
Momentum, P_K (GeV/c)

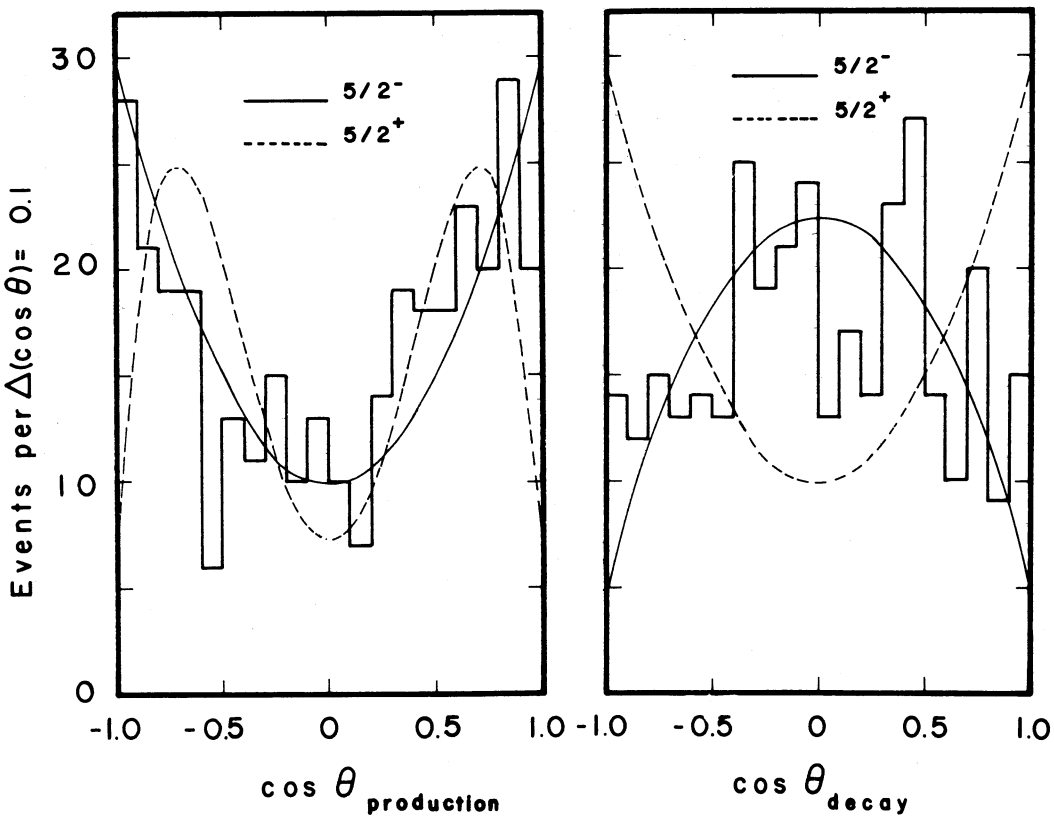
$5/2^-$
$5/2^+$
Events per $\Delta(\cos\theta) = 0.1$
$\cos\theta_{production}$
$\cos\theta_{decay}$

FIG. 18

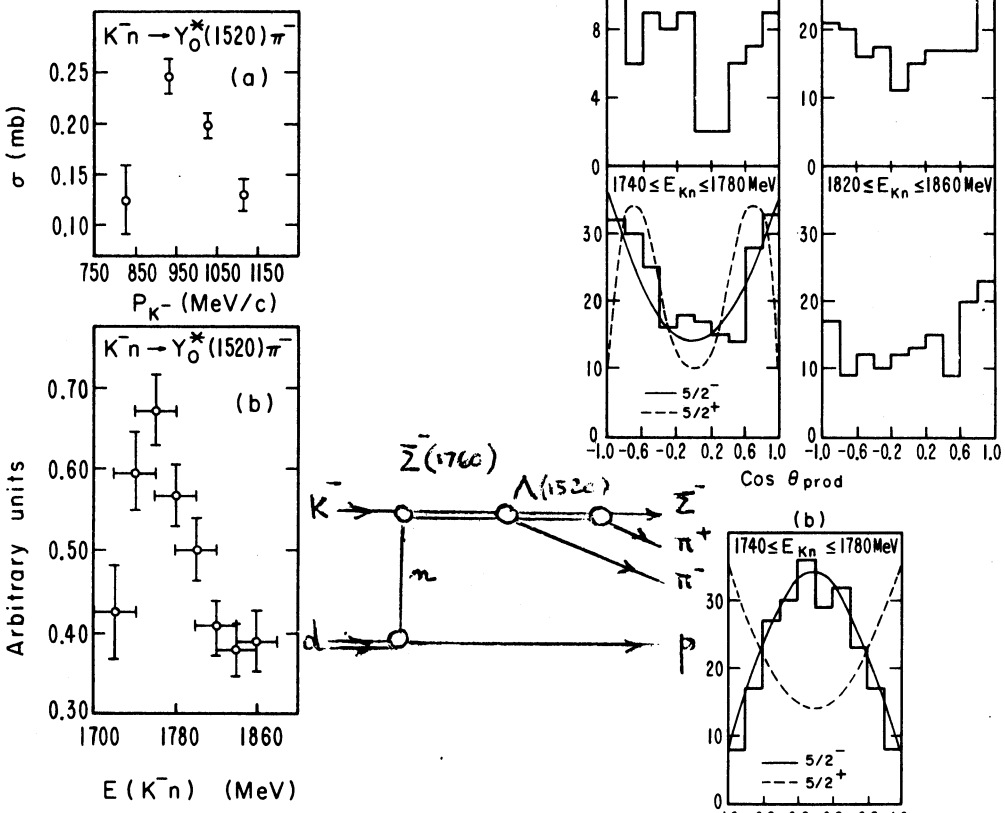

FIG. 2. (a) Cross sections for the reaction $K^- + n \to Y_0^*(1520)\pi^-$ at various incident momenta. (b) Ratio of the number of experimental events to the area under the theoretical K^-n c.m. energy distribution curve for the reaction $K^- + n \to Y_0^*(1520) + \pi^-$.

FIG. 3. (a) Production angular distributions for the $Y_0^*(1520)$. (b) Decay angular distribution of the $Y_0^*(1520)$ with respect to the production normal.

FIG. 19

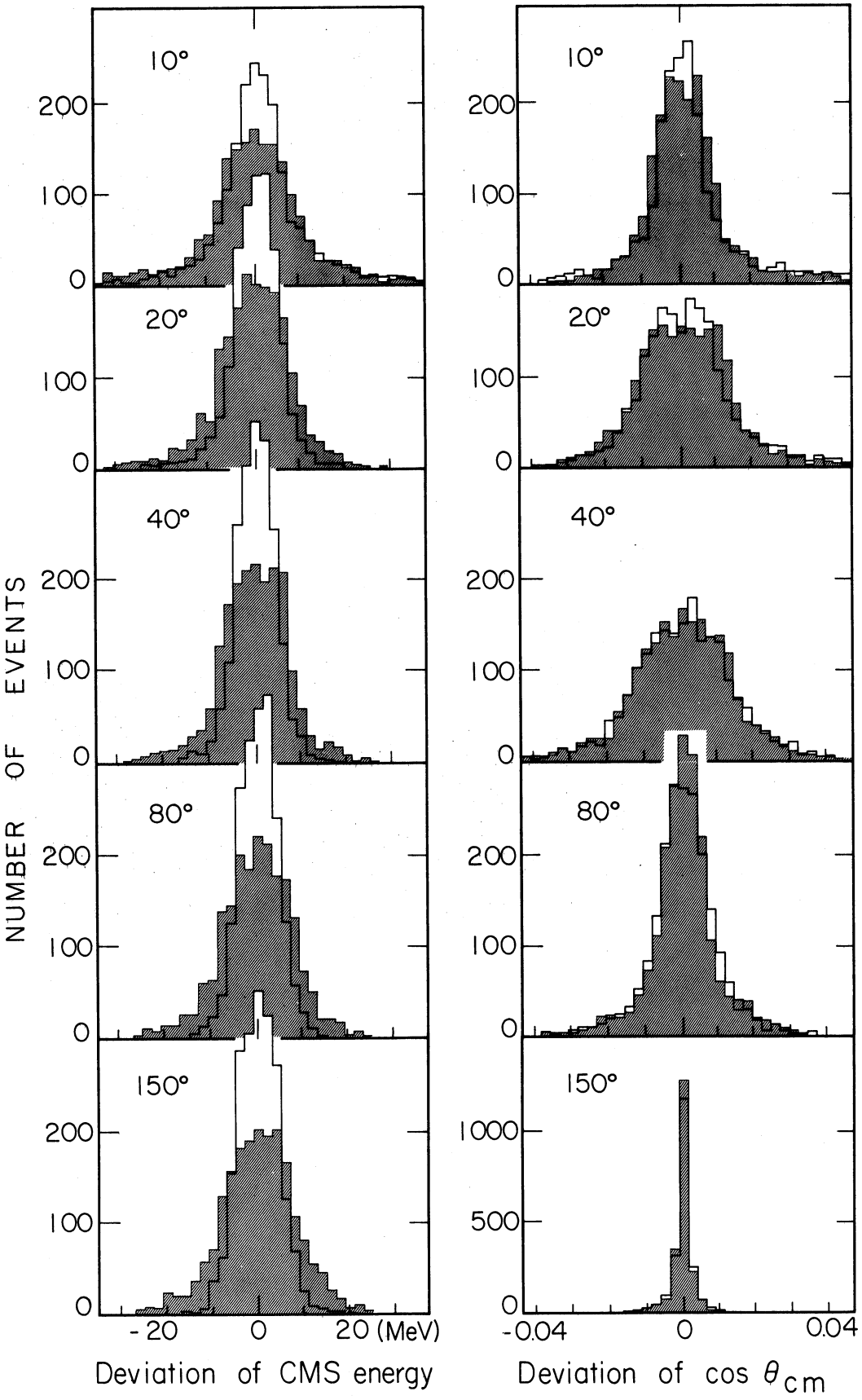
10°
20°
40°
80°
150°
200
100
0
1000
500
NUMBER OF EVENTS
-20
0
20 (MeV)
Deviation of CMS energy
-0.04
0
0.04
Deviation of cos θcm

FIG. 20

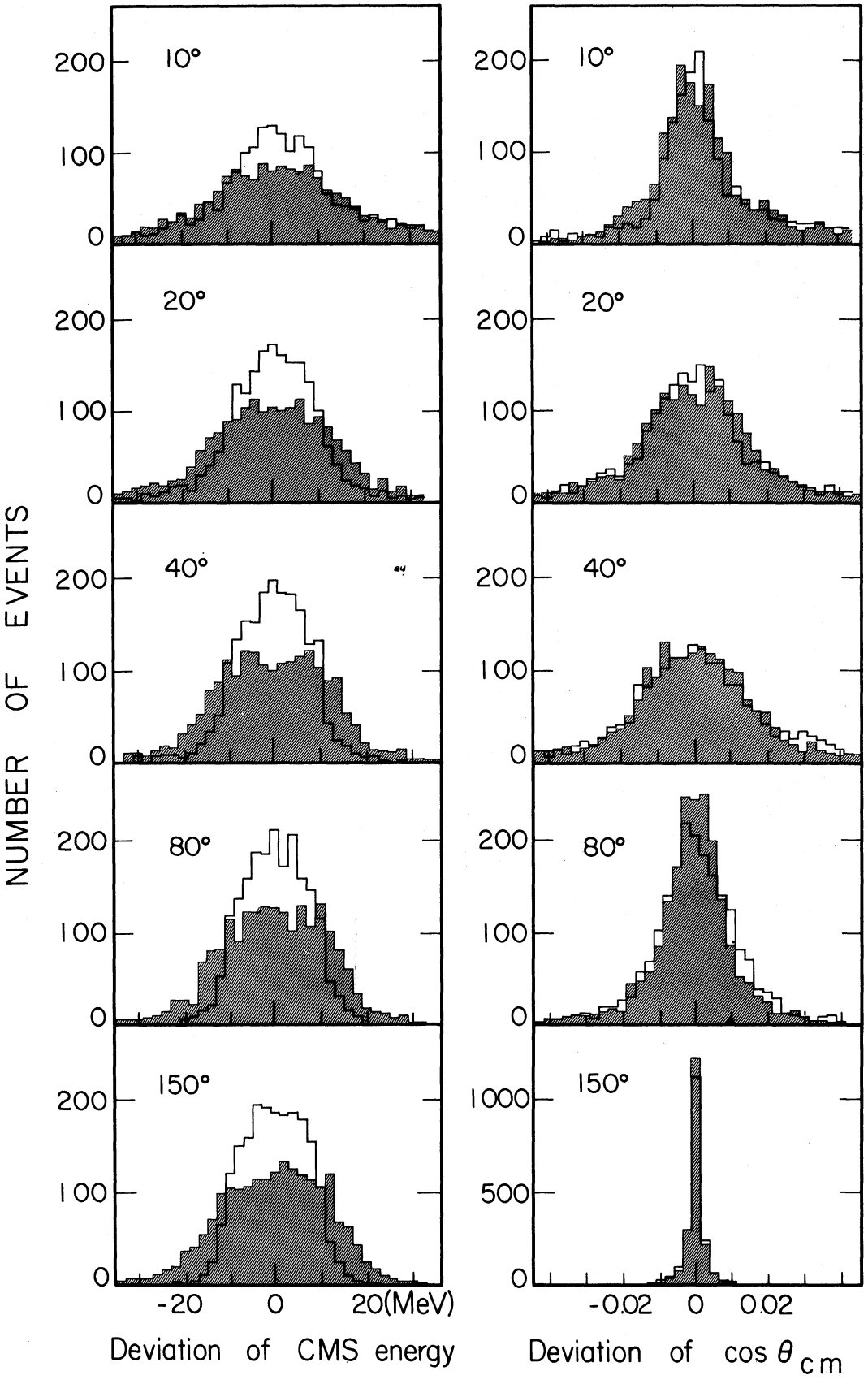
NUMBER OF EVENTS
10°
20°
40°
80°
150°
200
100
0
1000
500
-20
0
20(MeV)
-0.02
0
0.02
Deviation of CMS energy
Deviation of cos θ cm

FIG. 21

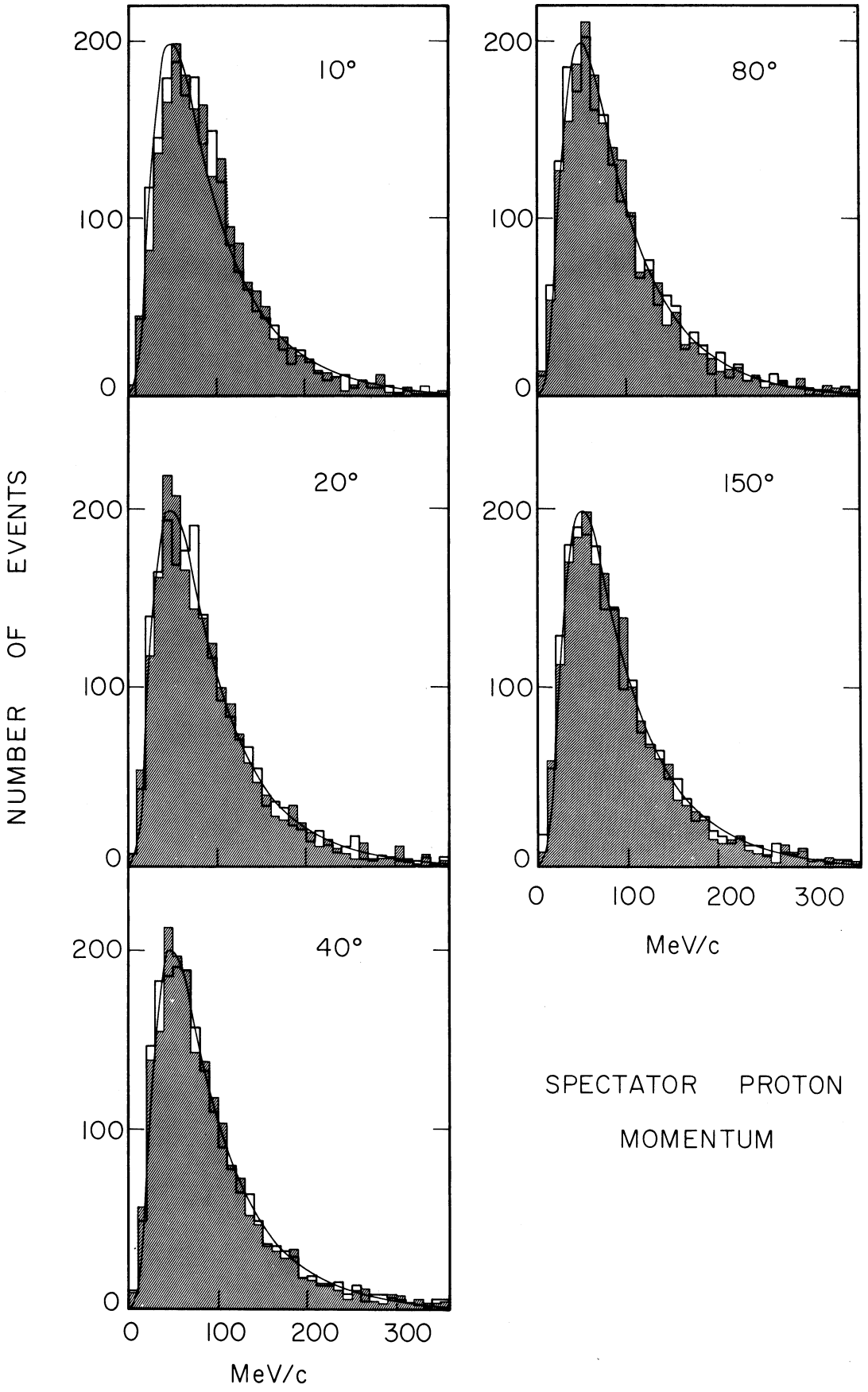
NUMBER OF EVENTS
200
100
0
10°
20°
40°
80°
150°
0
100
200
300
MeV/c
SPECTATOR PROTON
MOMENTUM

FIG. 22

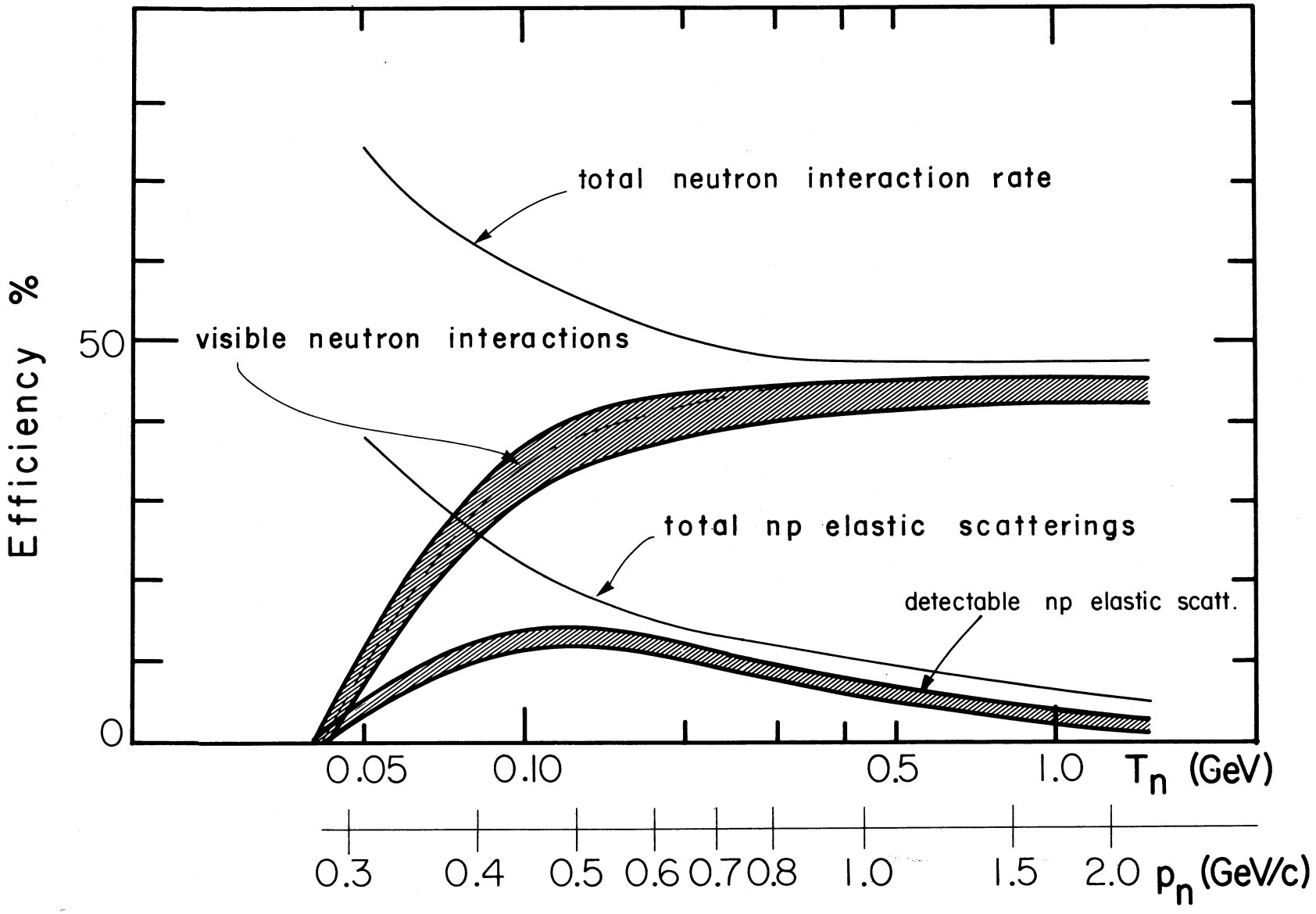
Efficiency %
50
0
total neutron interaction rate
visible neutron interactions
total np elastic scatterings
detectable np elastic scatt.
0.05
0.10
0.5
1.0
T_n (GeV)
0.3
0.4
0.5
0.6
0.7
0.8
1.0
1.5
2.0
p_n (GeV/c)

FIG. 23